



University of Pennsylvania
ScholarlyCommons

Departmental Papers (ESE)

Department of Electrical & Systems Engineering

2018

A Dynamical System for Prioritizing and Coordinating Motivations


Paul Reverdy

Electrical and Systems Engineering, University of Pennsylvania, preverdy@seas.upenn.edu

Daniel E. Koditschek

Electrical and Systems Engineering, University of Pennsylvania, kod@seas.upenn.edu

Follow this and additional works at: https://repository.upenn.edu/ese_papers

 Part of the [Electrical and Computer Engineering Commons](#), and the [Systems Engineering Commons](#)

Recommended Citation

Paul Reverdy and Daniel E. Koditschek, "A Dynamical System for Prioritizing and Coordinating Motivations", *SIAM J. Appl. Dyn. Syst* 17(2), 1683-1715. January 2018. <http://dx.doi.org/https://doi.org/10.1137/17M111972X>

This paper is posted at ScholarlyCommons. https://repository.upenn.edu/ese_papers/835

For more information, please contact repository@pobox.upenn.edu.

A Dynamical System for Prioritizing and Coordinating Motivations

Abstract

We develop a dynamical systems approach to prioritizing multiple tasks in the context of a mobile robot. We take navigation as our prototypical task, and use vector field planners derived from navigation functions to encode control policies that achieve each individual task. We associate a scalar quantity with each task, representing its current importance to the robot; this value evolves in time as the robot achieves tasks. In our framework, the robot uses as its control input a convex combination of the individual task vector fields. The weights of the convex combination evolve dynamically according to a decision model adapted from the bio-inspired literature on swarm decision making, using the task values as an input. We study a simple case with two navigation tasks and derive conditions under which a stable limit cycle can be proven to emerge. While moving along the limit cycle, the robot periodically navigates to each of the two goal locations; moreover, numerical study suggests that the basin of attraction is quite large so that significant perturbations are recovered with a reliable return to the desired task coordination pattern.

For more information: [Kod*lab](#) and <http://www.paulreverdy.com/2018/05/11/motivation-dynamics-simulations/>

Disciplines

Electrical and Computer Engineering | Engineering | Systems Engineering

A DYNAMICAL SYSTEM FOR PRIORITIZING AND COORDINATING MOTIVATIONS

PAUL REVERDY AND DANIEL E. KODITSCHKE*

Abstract. We develop a dynamical systems approach to prioritizing multiple tasks in the context of a mobile robot. We take navigation as our prototypical task, and use vector field planners derived from navigation functions to encode control policies that achieve each individual task. We associate a scalar quantity with each task, representing its current importance to the robot; this value evolves in time as the robot achieves tasks. In our framework, the robot uses as its control input a convex combination of the individual task vector fields. The weights of the convex combination evolve dynamically according to a decision model adapted from the bio-inspired literature on swarm decision making, using the task values as an input. We study a simple case with two navigation tasks and derive conditions under which a stable limit cycle can be proven to emerge. While flowing along the limit cycle, the robot periodically navigates to each of the two goal locations; moreover, numerical study suggests that the basin of attraction is quite large so that significant perturbations are recovered with a reliable return to the desired task coordination pattern.

Key words. limit cycles, geometric singular perturbation theory, relaxation oscillations, Hopf bifurcation

AMS subject classifications. 37G25, 37D10, 37N35

1. Introduction. A prototypical example of an autonomous system is a foraging animal that achieves its basic needs for food and shelter by periodically revisiting different locations in its environment at different times apparently governed by some internal sense of relative urgency or satiety. In the vocabulary of psychology, the animal can be said to have drives which motivate it to perform actions that reduce those drives [26, 10, 21]. Inspired by the flexibility and robustness of natural autonomous systems, we seek a simple model of their seemingly non-deliberative, drive-based decision-making mechanisms that might be robustly embodied within the dynamical sensorimotor layers of autonomous physical systems — a motivational dynamics for robots.

Dynamical systems approaches have been successful in understanding mechanisms for decision making in biological systems such as human choice behavior in two-alternative forced choice tasks [3], migration behavior in animal groups [17], and nest site selection behavior [24] in honeybee swarms. Often, these decision mechanisms are *value based* in the sense that the organism can be interpreted as associating a numerical value with each available alternative and selecting the alternative with the highest value. Decision making in biological systems tends to be embodied in the sense that animals implement their decisions by moving their bodies in some way. In the standard two-alternative forced choice task, an animal registers a decision by pushing a button or by looking at a particular point on a screen. In the context of migration or nest site selection, the animal moves its entire body to a new location. We take navigation, interpreted broadly as the task of steering a system to a desired goal state while avoiding obstacles, as the prototypical task for a mobile robot.

*Department of Electrical and Systems Engineering, University of Pennsylvania, Philadelphia, PA (preverdy@seas.upenn.edu, kod@seas.upenn.edu)

Vector field methods provide a natural way to encode the sensorimotor activity required to perform navigation tasks in dynamical systems language. When the vector field arises as the gradient of a well-chosen function, such as a navigation function [22], the system dynamics readily admit performance guarantees, such as proofs of convergence to the desired state while avoiding obstructions along the way. Furthermore, such vector field methods naturally map to control inputs for mechanical systems described by Lagrangian dynamics [13] and can be composed via linear combination or more intricate sequential [4] and parallel [5] operations. There have been exciting recent advances in logical approaches to dynamical task composition [14], but they introduce hybrid (even-based) transitions and require derived logical representation of the underlying dynamics. Instead, we seek an intrinsically dynamical systems approach to the composition and prioritization of potentially competing tasks that interprets the coefficients of their representative fields’ linear combinations as a kind of motivational state to be continuously adjusted in real time in a way that is flexible and robust to perturbations.

The main result of this paper is captured in Figure 1 which summarizes a numerical study illustrating two central analytical insights stated as Theorem 1 and Theorem 2. The motivational feedback path has a gain parametrized by $\epsilon_v > 0$ and a time scale parametrized by $\epsilon_\lambda > 0$. Numerical studies summarized by the four subsequent plots referenced by the numbered points of the figure indicate the presence of a stable limit cycle for a wide range of these parameter values. Analysis reveals that ϵ_v plays the role of an ϵ_λ -dependent bifurcation parameter. Specifically, in the fast timescale limit $\epsilon_\lambda \rightarrow 0$, Theorem 1 establishes the existence of a Hopf bifurcation at a critical value of the feedback gain parameter $\epsilon_v^*(0)$. Further numerical study confirms the value of that formally-determined parameter, and suggests that the Hopf bifurcation persists along a curve of critical values, $\epsilon_v^*(\epsilon_\lambda)$ for positive ϵ_λ .

Seeking formal confirmation of the limit cycles suggested by those simulations at the physically interesting parameter values where $\epsilon_\lambda > 0$, we next take recourse to a singular perturbation analysis. Specifically, we consider the joint limit $\epsilon_v \rightarrow 0, \epsilon_\lambda \rightarrow 0$ and carry out a dimension reduction of the system in this limit yielding planar dynamics exhibiting a limit cycle established by application of the Poincaré-Bendixson theorem. Arguments from geometric singular perturbation theory together with its conjectured (numerically corroborated) hyperbolicity then imply that this limit cycle persists for finite $\epsilon_v, \epsilon_\lambda > 0$.

This work is related to prior literature on dynamical decision-making in biological systems. Seeley *et al.* [24] studied nest site selection behavior in honeybee swarms and discovered a mechanism called a stop signal, by which bees who were committed to one nest site physically wrestled bees committed to other sites in order to get them to abandon their commitment. Seeley *et al.* constructed a dynamical systems model of this behavior and showed that the introduction of a stop signal allowed the system to avoid the deadlock state where no clear majority emerges in favor of any given option. We use the dynamical system from Seeley *et al.* [24] which models value-based nest site selection in honeybee swarms to modulate the motivation state. We let the value associated with each task be modulated by how far the agent is from the goal state associated with that task. This introduces feedback into the motivation dynamics by making the current system state influence the task values and thereby the motivation state.

Pais *et al.* [20] studied Seeley *et al.*’s model [24] using singular perturbation theory and showed that the stop signal also makes the model sensitive to the absolute value of the alternatives, allowing the system to remain in deadlock if all alternatives are

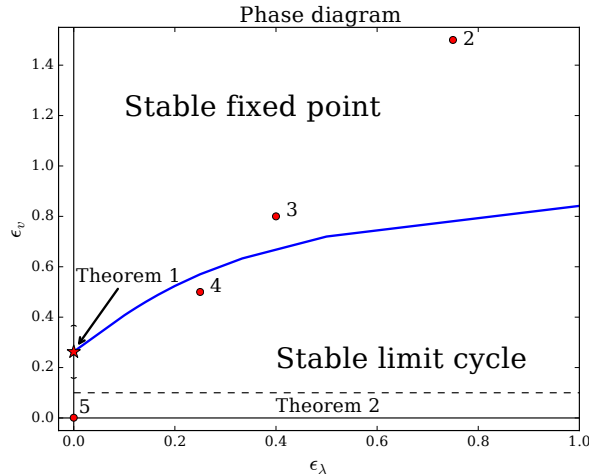


FIG. 1. In blue, we see the bifurcation value $\epsilon_v^*(\epsilon_\lambda)$ numerically computed for a variety of values of ϵ_λ . Simulations run with parameter values above the line exhibit a stable deadlock equilibrium, while values below the line exhibit oscillatory behavior. The red circles represent the values taken in the simulations displayed in succeeding figures with the corresponding number. Corroborating these numerical observations we establish the following formal results. In the single limit $\epsilon_\lambda \rightarrow 0$, Theorem 1 establishes a Hopf bifurcation at $\epsilon_{v,0} \approx 0.262$, guaranteeing a family of stable limit cycles in a small (one-dimensional) neighborhood of ϵ_v values (at the $\epsilon_\lambda = 0$ limit) around the red star. In the joint limit $\epsilon_\lambda, \epsilon_v \rightarrow 0$, Theorem 2 uses a singular perturbation argument to establish the persistence of stable limit cycles in some neighborhood of the abscissa of this plot.

equally poor. Pais *et al.* suggested that this sensitivity is useful to avoid prematurely committing to a suboptimal alternative, and show that it results in hysteresis as a function of the difference in the value of the alternatives. These convincing accounts of the utility and potential analytical tractability of such bioinspired decision models provide a direct point of departure for our work. Specifically, [20, 24] studied one-off decisions where the value of each option (i.e., task) is static. In contrast, we allow the values of the tasks to change dynamically as they are completed by feeding back the system state, which allows the agent to determine the status of each task.

Other authors, particularly in the evolutionary dynamics literature, have studied systems with similar types of feedback. In evolutionary dynamics [9], which seeks to formalize Darwin’s ideas about natural selection, a set of populations each representing different strategies interact with each other and the interaction determines the level of fitness of each strategy. Fit populations thrive and grow, while unfit populations die off. Pais, Caicedo, and Leonard [19] studied the replicator-mutator equations from evolutionary dynamics with a particular network structure to the fitness function and showed conditions under which the dynamics exhibit Hopf bifurcations resulting in limit cycles. Mitchener and Nowak [18] studied evolutionary dynamics as a model of language transmission and showed conditions under which the dynamics of distinct grammars can exhibit limit cycles corresponding to periodic changes in the dominant grammar. The feedback model adopted by [19] and [18] captures the evolutionary process in which the fitness of a given strategy is determined by the relative fractions of the population adopting that strategy. Such a model is inappropriate for our robotic application, where the value of a task need not arise from competitive interactions between tasks. Our Hopf analysis in Section 4 is similar to that in [19], but we go on

to show the existence of limit cycles in a two-dimensional region in parameter space using tools from geometric singular perturbation theory.

The remainder of the paper is structured as follows. In Section 2 we lay out the broad class of systems under consideration before specifying the instance of the model which we study and stating our formal results. In Section 3 we show the result of several illustrative simulations, which suggest the existence of a Hopf bifurcation. In Section 4 we study the system in the limit $\epsilon_\lambda \rightarrow 0$ and show the existence of a Hopf bifurcation that results in stable limit cycles. In Section 5 we study the system in the joint limit $\epsilon_\lambda \rightarrow 0, \epsilon_v \rightarrow 0$ and show the existence of a stable limit cycle in the resulting two-dimensional reduced system; in Section 6 we show that this limit cycle persists for finite values of ϵ_v and ϵ_λ . Finally, we conclude in Section 7.

2. Model, Problem Statement, and Formal Results. In this section we define our system model, state the problem we address and the formal results we obtain.

2.1. Model. Our model consists of three interconnected dynamical subsystems: states representing the navigation tasks and associated control actions (vector fields); the motivation state m ; and the value state v . Implicit in the definition of the navigation tasks is the definition of the physical agent, which comprises the agent’s body and its workspace, or environment.

2.1.1. Body, Environment, and Motivational States. We model the robot as a point particle located at $x \in \mathcal{D}$, where the environment $\mathcal{D} \subseteq \mathbb{R}^d$ is a domain within Euclidean space. In general, \mathcal{D} may be punctured by obstacles, but in this initial work we restrict ourselves to unobstructed domains.

We represent *motivation* by the state $m \in \Delta^N$, where $\Delta^N = \{m \in \mathbb{R}^{N+1} : m_i \geq 0, \sum_{i=1}^{N+1} m_i = 1\}$ is the N -simplex. We index the first N elements of m by $i \in \{1, \dots, N\}$: m_i represents the motivation to perform task i . The last element we label as m_U : this represents undecided motivation, i.e., the decision to not perform any task.

2.1.2. Tasks. The agent has a set of N tasks. Each task $i \in \{1, \dots, N\}$ requires navigating the agent to the location $x_i^* \in \mathcal{D}$. For each task i , we assume the existence of a navigation function [22] $\varphi_i : \mathcal{D} \rightarrow [0, 1]$. The navigation function yields a gradient field $-\nabla\varphi_i$ such that $\dot{x} = -\nabla\varphi_i$ obeys

$$\lim_{t \rightarrow +\infty} x(t) = x_i^*.$$

That is, the gradient field $-\nabla\varphi_i$ is a vector field that accomplishes task i . In the following, where the domain is assumed to be unobstructed, we define the navigation functions by the Euclidean distance

$$(1) \quad \varphi_i(x) = \|x - x_i^*\|_2,$$

Since the gradient field $\nabla\varphi_i = (x - x_i^*)/\|x - x_i^*\|$ is not Lipschitz in the neighborhood of $x = x_i^*$, we introduce the scaled navigation vector fields

$$(2) \quad f_{n,i}(x) := -\text{sat}(\varphi_i(x), \eta)\nabla\varphi_i(x), \quad i \in \{1, \dots, N\},$$

where sat is the saturation function

$$\text{sat}(y, \eta) := y/|y|_\eta := y/\sqrt{y^2 + \eta^2},$$

where $|x|_\eta = \sqrt{x^2 + \eta^2}$ is a thresholded absolute value and $1 \gg \eta > 0$. For the remainder of the paper we set $\eta = 10^{-6}$. It is clear that the scaling leaves the asymptotic properties of the navigation dynamics unchanged.

Finally, we define the matrix-valued function consisting of the N task navigation vector fields plus the null gradient field associated with indecision

$$(3) \quad \Phi(x) = [f_{n,1}(x) \quad \dots \quad f_{n,N}(x) \quad 0] \in \mathbb{R}^{d \times (N+1)}.$$

By taking convex combinations of these vector fields we can assign the agent weighted combinations of the instantaneous (“greedy”) task plans they represent; the motivation state, defined below, will specify the convex combination to be taken at any given time.

The agent’s high-level mission is to repeatedly carry out each of the N low-level tasks, i.e., visit each of the N locations, in a specified order. In the vocabulary of the LTL hybrid systems literature, this corresponds to a recurrent patrol or coverage mission. We now develop the detailed model, introducing its states and dynamics, then finally present statements of the problem we address and the formal results.

2.2. Model Dynamics. Having specified the system model and its state space, we now define its dynamics. The system has state $(x, m, v) \in \mathcal{D} \times \Delta^N \times \mathbb{R}_+^N$. The state variables evolve according to the dynamics

$$(4) \quad \dot{x} = f_x(x, m)$$

$$(5) \quad \dot{m} = f_m(m, v)$$

$$(6) \quad \dot{v} = f_v(v, x).$$

The specific forms of the functions f_x , f_m , and f_v are given in the following paragraphs.

2.2.1. Navigation dynamics. The body’s location dynamics are the convex combination of the N navigation vector fields (plus the null field associated with indecision), weighted by the motivation state:

$$(7) \quad \dot{x} = f_x(x, m) = -m^T \Phi(x).$$

For example, when $m = [1, 0, \dots, 0]$, the navigation dynamics are $\dot{x} = -m^T \Phi(x) = -\text{sat}(\varphi_1(x), \eta) \nabla \varphi_1(x)$, and when $m = [0, \dots, 0, 1]$, the dynamics are $\dot{x} = 0$.

2.2.2. Motivation dynamics. We take the motivation state dynamics from Pais *et al.*’s work [20] studying group decision making behavior in honeybee swarms:

$$(8) \quad \dot{m}_i = \tilde{v}_i m_U - m_i (1/\tilde{v}_i - \tilde{v}_i m_U + \sigma_i (1 - m_i - m_U)).$$

We set $\tilde{v}_i = v_i^* v_i$, where $v_i \in [0, 1]$ is the normalized value of task i and $v_i^* > 0$ is a gain parameter that scales v_i . Equation (8) holds for each $i \in \{1, \dots, N\}$, with the dynamics for m_U following from the constraint that defines the simplex.

The dynamics (8) were derived for group decision making in [24] from a microscopic individual-level Markov process model that incorporates commitment, abandonment, recruitment, and stop signal mechanisms. The term $\tilde{v}_i m_U$ represents spontaneous commitment of an uncommitted individual to option i at a rate which is proportional to the value \tilde{v}_i , $-m_i/\tilde{v}_i$ represents spontaneous abandonment, $\tilde{v}_i m_i m_U$ represents recruitment of an uncommitted individual by one committed to option i , and $-\sigma_i m_i (1 - m_i - m_U)$ represents a signal from individuals committed to options other than i telling individuals committed to option i to abandon their commitment.

In our context where m represents a single decision maker’s motivation state, each of these mechanisms can be interpreted as modeling specific processes between neurons in the decision maker’s brain rather than between individuals in a group.

2.2.3. Value dynamics. We define the value state dynamics as

$$(9) \quad \begin{aligned} \dot{v}_i &= \lambda_i(1 - v_i) - \lambda_i(1 - \varphi_i(x)) \\ &= \lambda_i(\varphi_i(x) - v_i), i \in \{1, \dots, N\}, \end{aligned}$$

Each v_i lies in the interval $[0, 1]$. Recall that the navigation functions φ_i are defined such that they tend to unity far from the goal x_i^* and take the value zero at the goal. The first term causes the value v_i to drift upwards towards unity, while the second term causes the value to decay when the goal x_i^* is reached (and $\varphi_i(x)$ tends to zero). Both dynamics are exponential with time scale λ_i . The dynamics (9) corresponds closely to the concept of drive reduction theory in social psychology, where motivation is thought to arise from the desire to carry out actions that satisfy various intrinsic drives [26, 10].

2.3. Formal Problem Statement and Analytical Results. The foregoing presentation introduces a broad class of models whose application to specific problems of reactive task planning and motivational control of multiple competing tasks we intend to explore empirically on physical robots. For the analytical purposes of this paper we find it expedient to consider a severely restricted instance from that class entailing only two, greatly simplified tasks and affording, in turn, a low-dimensional parametrization through imposition of various symmetries. In this section we first introduce the details of that restricted problem class and then state the analytical results we obtain.

2.3.1. Two Tasks, Their Essential Parameters, and New Coordinates.

We have four parameters for each task $i \in \{1, \dots, N\}$. Each task requires navigating to a goal location $x_i^* \in \mathcal{D}$. In the motivation dynamics (8), there is a positive stop signal parameter $\sigma_i > 0$ and value gain $v_i^* > 0$. Finally, in the value dynamics (9), there is a time scale $\lambda_i > 0$. We show that the number of parameters can be greatly reduced and that the system’s behavior can be largely understood by varying the value of v_i^* .

For many parameter values, the system (7)–(9) exhibits a stable limit cycle in numerical simulations. To systematically study the system, we specialize to the case of a planar workspace $\mathcal{D} = \mathbb{R}^2$ and $N = 2$ tasks. Then the state space of the system (7)–(9) is $\mathbb{R}^2 \times \Delta^2 \times [0, 1]^2$, for which we pick the coordinates $\xi = (x_1, x_2, m_1, m_2, v_1, v_2)$. Furthermore, we set the following parameter values.

We set the two goal locations to $x_1^* = (l, 0) \in \mathcal{D}$, $x_2^* = (0, l) \in \mathcal{D}$. This choice is made without loss of generality, as it amounts to a translation and rotation of the coordinates x for \mathcal{D} . The distance between the goal locations defines a length scale $\|x_1^* - x_2^*\|_2 = \sqrt{2}l := c$ which remains a free parameter. We set the nominal value of c to unity; again, this results in no loss of generality since it amounts to a scaling of the coordinates. For the stop signal σ_i , we follow Pais *et al.* [20] and impose the symmetry $\sigma_1 = \sigma_2 = \sigma$. Pais *et al.* set $\sigma = 4$, which we adopt as our nominal value. Similarly, for ease of exposition and analysis we equate the value gain parameters $v_1^* = v_2^* = v^* > 0$ as well as the value time scale parameters $\lambda_1 = \lambda_2 = \lambda > 0$. With these choices the set of system parameters is reduced to c, σ, v^* , and λ , each of which must be positive. Fixing c and σ at their nominal values of 1 and 4, respectively, leaves v^* and λ as free parameters whose values determine the behavior of the system.

In the case $N = 2$ and assuming φ_i defined by (1), the equations (7)–(9) are

$$(10) \quad \dot{\zeta} = f_\zeta(\zeta),$$

where the components of f_ζ are given by

$$\begin{aligned} \dot{x} &= -m_1 \operatorname{sat}(\varphi_1(x), \eta) \frac{x - x_1^*}{\|x - x_1^*\|_2} - m_2 \operatorname{sat}(\varphi_2(x), \eta) \frac{x - x_2^*}{\|x - x_2^*\|_2} \\ \dot{m}_1 &= (v^* v_1) m_U - m_1 (1/(v^* v_1) - (v^* v_1) m_U + \sigma m_2) \\ \dot{m}_2 &= (v^* v_2) m_U - m_2 (1/(v^* v_2) - (v^* v_2) m_U + \sigma m_1) \\ \dot{v}_1 &= \lambda(\varphi_1(x) - v_1) \\ \dot{v}_2 &= \lambda(\varphi_2(x) - v_2). \end{aligned}$$

Let $e_1 = x_1^* - x_2^*$ and let $e_2 \in \mathbb{R}^2$ be orthogonal to e_1 . Then $P = \{x \in \mathbb{R}^2 \mid x = x_1^* + \alpha e_1, \alpha \in \mathbb{R}\}$ is the line in \mathbb{R}^2 that passes through the points $x_1^*, x_2^* \in \mathbb{R}^2$. Equivalently, P can be expressed as the level set $f_p(x) = 0$, where $f_p(x) := e_2^T(x - x_1^*)$. For $x \in P$, we have $e_2^T(x - x_2^*) = e_2^T(x - x_2^* + (x_1^* - x_2^*)) = e_2^T(x - x_1^* + e_1) = f_p(x) + e_2^T e_1 = 0$. The set P is positively invariant, since for $x \in P$, we have

$$\begin{aligned} \dot{f}_p &= e_2^T(\dot{x}) = e_2^T(-m_1(x - x_1^*)/|\varphi_1(x)|_\eta - m_2(x - x_2^*)/|\varphi_2(x)|_\eta) \\ &= -e_2^T(x - x_1^*)m_1/|\varphi_1(x)|_\eta - e_2^T(x - x_2^*)m_2/|\varphi_2(x)|_\eta = 0. \end{aligned}$$

Therefore, x cannot cross the line P , which divides the plane, and x is constrained to remain in the half of the plane where it was initially. We denote this closed half plane by $H_0 \subset \mathbb{R}^2$. The navigation functions $(\varphi_1(x), \varphi_2(x))$ are coordinates for the plane. The transformation $H_0 \rightarrow \mathbb{R}_+^2$ defined by $x \mapsto (\varphi_1, \varphi_2)$ is a bijection and it is easily verified that it is a diffeomorphism. Therefore, without loss of generality we can restrict the dynamics to the space $H_0 \times \Delta^2 \times [0, 1]^2$ with the coordinates $\zeta = (\varphi_1, \varphi_2, m_1, m_2, v_1, v_2)$.

We make one further change of coordinates by transforming into mean and difference coordinates defined by

$$\Delta\varphi = \varphi_1 - \varphi_2, \bar{\varphi} = \frac{\varphi_1 + \varphi_2}{2}$$

and likewise for $\Delta m, \bar{m}, \Delta v$, and \bar{v} . Define the coordinates

$$(11) \quad z = (\Delta\varphi, \bar{\varphi}, \Delta m, \bar{m}, \Delta v, \bar{v})$$

on the space $[-1, 1] \times \mathbb{R}_+ \times \Delta^2 \times [0, 1]^2$ and parameters $\epsilon_v = 1/v^*$ and $\epsilon_\lambda = 1/\lambda$. It is easy to see that the transformation from ζ to z is a diffeomorphism. (In fact $(\Delta\varphi, \bar{\varphi})$ are elliptic coordinates for H_0 that are related to the standard elliptic coordinates (σ, τ) [25] by $\bar{\varphi} = \sigma, \Delta\varphi = c\tau$.) In the mean-difference coordinates, the dynamics (10) are

$$(12) \quad \dot{z} = f_z(z),$$

where the components of f_z are given by

$$(13) \quad \begin{aligned} \dot{\Delta\varphi} = f_{\Delta\varphi}(z) &= \frac{\Delta\varphi^2 - 1}{(4\bar{\varphi}^2 - \Delta\varphi^2)^2} \\ &\times \left((2\bar{m} + \Delta m)(2\bar{\varphi} + \Delta\varphi)^2 \operatorname{sat}(2\bar{\varphi} + \Delta\varphi, 2\eta) \right. \\ &\quad \left. - (2\bar{m} - \Delta m)(2\bar{\varphi} - \Delta\varphi)^2 \operatorname{sat}(2\bar{\varphi} - \Delta\varphi, 2\eta) \right), \end{aligned}$$

$$(14) \quad \dot{\varphi} = f_{\varphi}(z) = -\frac{1}{2} \frac{4\bar{\varphi}^2 - 1}{(4\bar{\varphi}^2 - \Delta\varphi^2)^2} \times \left((2\bar{m} + \Delta m)(2\bar{\varphi} + \Delta\varphi)^2 \text{sat}(2\bar{\varphi} - \Delta\varphi, 2\eta) + (2\bar{m} - \Delta m)(2\bar{\varphi} - \Delta\varphi)^2 \text{sat}(2\bar{\varphi} + \Delta\varphi, 2\eta) \right),$$

$$(15) \quad \Delta\dot{m} = f_{\Delta m}(z) = -\epsilon_v \left(\frac{2\bar{m} + \Delta m}{2\bar{v} + \Delta v} - \frac{2\bar{m} - \Delta m}{2\bar{v} - \Delta v} \right) + \bar{v}\Delta m(1 - 2\bar{m})/\epsilon_v + \Delta v(1 - 2\bar{m})(1 + \bar{m})/\epsilon_v,$$

$$(16) \quad \dot{m} = f_{\bar{m}}(z) = \frac{1}{2} \left(-\epsilon_v \frac{2\bar{m} + \Delta m}{2\bar{v} + \Delta v} - \epsilon_v \frac{2\bar{m} - \Delta m}{2\bar{v} - \Delta v} + \frac{2\bar{v} + \Delta v}{2\epsilon_v} (1 - 2\bar{m}) \left(1 + \frac{2\bar{m} + \Delta m}{2} \right) + \frac{2\bar{v} - \Delta v}{2\epsilon_v} (1 - 2\bar{m}) \left(1 + \frac{2\bar{m} - \Delta m}{2} \right) - \frac{\sigma}{2} (2\bar{m} + \Delta m)(2\bar{m} - \Delta m) \right),$$

$$(17) \quad \epsilon_{\lambda} \dot{\Delta v} = f_{\Delta v}(z) = -(\Delta v - \Delta\varphi),$$

$$(18) \quad \epsilon_{\lambda} \dot{\bar{v}} = f_{\bar{v}}(z) = -(\bar{v} - \bar{\varphi}).$$

2.3.2. Formal Results. In this section we state the two theorems which constitute the formal results of the paper. As can be seen in the simulations presented in Section 3, the dynamics (12) appear to exhibit a Hopf bifurcation as the parameters ϵ_v and ϵ_{λ} approach zero, giving birth to stable limit cycles. We formalize this observation in two steps. First we consider the limit $\epsilon_{\lambda} \rightarrow 0$ which reduces the dimension of the system (12) and permits an explicit computation showing the existence of a Hopf bifurcation.

In the limit $\epsilon_{\lambda} \rightarrow 0$, the v dynamics are directly coupled to the φ dynamics, so $\Delta v = \Delta\varphi$ and $\bar{v} = \bar{\varphi}$, which are fixed points of Equations (17) and (18), respectively. Define $z_r = (\Delta\varphi, \bar{\varphi}, \Delta m, \bar{m})$ as the vector of the remaining state variables. Explicitly, z and z_r are related by the linear embedding $z = h(z_r)$ with left inverse given by the linear projection h^{\dagger} , where

$$h(z_{r,1}, z_{r,2}, z_{r,3}, z_{r,4}) := (z_{r,1}, z_{r,2}, z_{r,3}, z_{r,4}, z_{r,1}, z_{r,2}); \quad h^{\dagger}(z) := (z_1, z_2, z_3, z_4)$$

Then the dynamics (12) reduce to the restriction dynamics

$$(19) \quad \dot{z}_r = f_r(z_r, \epsilon_v) := Dh^{\dagger} \cdot f_z \circ h(z_r),$$

The restriction dynamics exhibit a Hopf bifurcation, as summarized in the following theorem:

THEOREM 1. *Set $\sigma = 4$. The system $\dot{z}_r = f_r(z_r, \epsilon_v)$ defined by (19) has a deadlock equilibrium z_{rd} given by (22). For sufficiently small $\eta > 0$, the dynamics undergo a Hopf bifurcation resulting in stable periodic solutions at $(z_{rd}, \epsilon_{v,0}(\eta))$, where $\eta \ll 1$ is the saturation constant. In the limit $\eta \rightarrow 0$, $\epsilon_{v,0}(0) \approx 0.262$ is the smaller of the two real-valued solutions of $(1 - 4\epsilon_v^2)^2 - 2\epsilon_v = 0$.*

As we are ultimately motivated by the physically meaningful case of small but non-zero values of ϵ_v and ϵ_λ , we study the singular perturbation limit $\epsilon_v, \epsilon_\lambda \rightarrow 0$ under which the system (12) can be reduced to a planar dynamical system and show the existence of a limit cycle. We then employ tools from geometric singular perturbation theory to show the persistence of this limit cycle for sufficiently small, but finite, values of ϵ_v and ϵ_λ :

THEOREM 2. *Accepting Conjecture 21, below, for $\sigma = 4$, there exists a stable limit cycle of (12) for sufficiently small, but finite, values of ϵ_λ and ϵ_v . Equivalently, fixing λ , there exists a stable limit cycle of (12) for sufficiently large, but finite, values of v^* .*

3. Illustrative Simulations. Figure 1 summarizes the behavior of the system (12) as a function of the two parameters ϵ_v and ϵ_λ . For large values of both parameters, the system exhibits a stable deadlock equilibrium, while for sufficiently small values of both parameters the system exhibits a stable limit cycle composed of a slow segment followed by a fast jump, which is characteristic of relaxation oscillations [2, 7]. Section 4 studies the system in the limit $\epsilon_\lambda \rightarrow 0$ and analytically shows the existence of a Hopf bifurcation at $\epsilon_v = \epsilon_{v,0} \approx 0.262$. The blue line in Figure 1 shows the numerically-computed bifurcation value $\epsilon_v^*(\epsilon_\lambda)$ for $\epsilon_\lambda > 0$. The numerically-computed limit $\lim_{\epsilon_\lambda \rightarrow 0} \epsilon_v^*(\epsilon_\lambda)$ corresponds well to the analytical value $\epsilon_{v,0}$.

Figures 2–5 show simulations of the system (12) for four representative values of the parameters $\epsilon_v, \epsilon_\lambda$. We set $\sigma = 4$. In ξ coordinates, the initial conditions were $x = 0, m_1 = 0, m_2 = 1/2, v_1 = v_2 = 0.1$. In the mean-difference coordinates z this corresponds to $\Delta\varphi = 0, \bar{\varphi} = \sqrt{2}/2, \Delta m = -1/2, \bar{m} = 1/4, \Delta v = 0$, and $\bar{v} = 0.1$. This choice of initial conditions was made to avoid the deadlock equilibrium but was otherwise generic.

Figure 2 suggests that for large values of $\epsilon_v, \epsilon_\lambda$ there is a stable deadlock equilibrium in the system where no oscillations are present. Analyzing the dynamics, we see that this equilibrium corresponds to the state $z_d = (\Delta\varphi_d, \bar{\varphi}_d, \Delta m_d, \bar{m}_d, \Delta v_d, \bar{v}_d)$, where $\bar{\varphi}_d = 1/2, \bar{v}_d = \bar{\varphi}_d = 1/2, \Delta\varphi_d = \Delta m_d = \Delta v_d = 0$, and \bar{m}_d solves the following quadratic equation:

$$(20) \quad -2(1 + \sigma\epsilon_v)\bar{m}_d^2 - (4\epsilon_v^2 + 1)\bar{m}_d + 1 = 0,$$

which has the solution $\bar{m}_d(\epsilon_v)$ given by

$$(21) \quad \frac{-(4\epsilon_v^2 + 1) + \sqrt{(4\epsilon_v^2 + 1)^2 + 8(1 + \sigma\epsilon_v)}}{4(1 + \sigma\epsilon_v)} \\ = \frac{-(4\epsilon_v^2 + 1) + \sqrt{16\epsilon_v^4 + 8\epsilon_v^2 + 8\sigma\epsilon_v + 9}}{4(1 + \sigma\epsilon_v)},$$

which is clearly positive, as σ and ϵ_v are both positive, which implies that the second term under the radical in (21) is positive. Figures 2–5 suggest that the system undergoes a Hopf bifurcation as the parameters ϵ_v and ϵ_λ are decreased. In the following sections we carry out a series of analyses to characterize the bifurcation and study the resulting limit cycle.

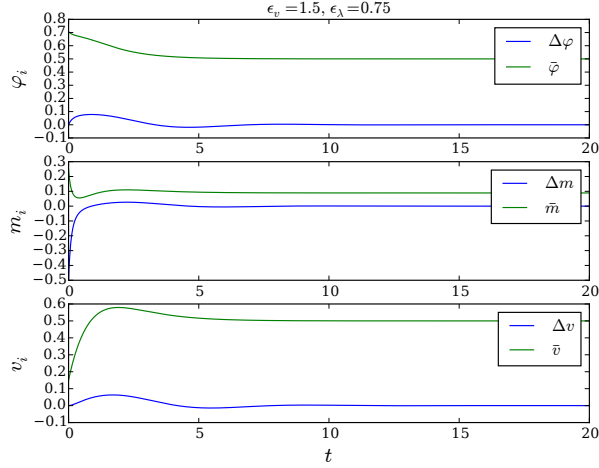


FIG. 2. Large values of both scales, represented by $\epsilon_v = 1.5, \epsilon_\lambda = 0.75$. The system converges to a stable deadlock equilibrium and no oscillations are present.

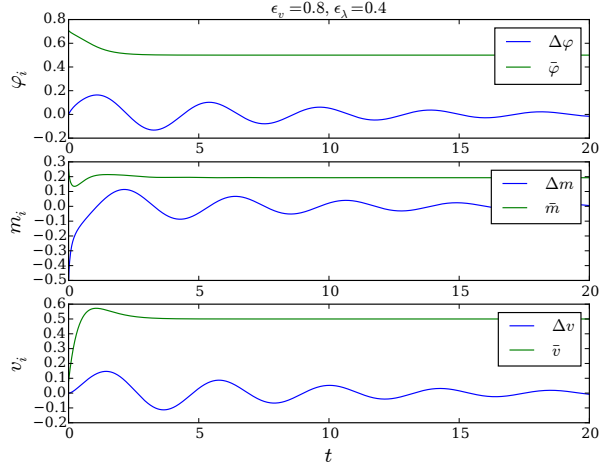


FIG. 3. Parameter values $\epsilon_v = 0.8, \epsilon_\lambda = 0.4$ that are near the Hopf bifurcation but still in the stable fixed point regime. The system displays damped oscillatory behavior that appears nearly linear, as to be expected near a Hopf bifurcation.

4. Hopf analysis in the limit $\epsilon_\lambda \rightarrow 0$. Motivated by the numerical evidence of a Hopf bifurcation occurring at the deadlock equilibrium, we consider the system (12) in the limit $\epsilon_\lambda \rightarrow 0$ and analytically show the existence of a Hopf bifurcation in this limiting case as ϵ_v is lowered through a critical value $\epsilon_{v,0}$. We then numerically consider the case of finite ϵ_λ and compute the bifurcation value $\epsilon_v^*(\epsilon_\lambda)$ for a range of values of ϵ_λ ; the numerically-computed limit $\lim_{\epsilon_\lambda \rightarrow 0} \epsilon_v^*(\epsilon_\lambda)$ matches the analytical result $\epsilon_{v,0}$, as shown in Figure 1.

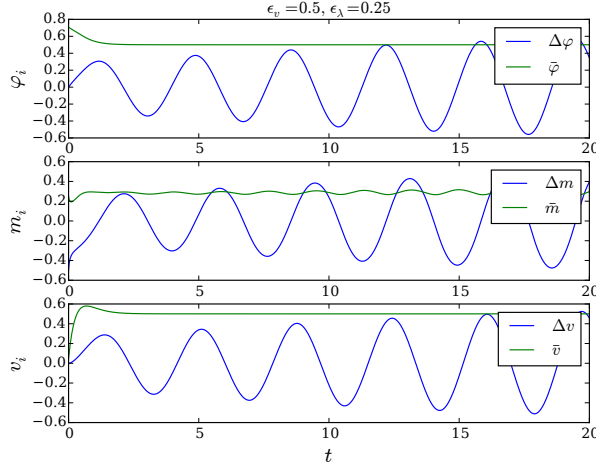


FIG. 4. Parameter values $\epsilon_v = 0.5, \epsilon_\lambda = 0.25$ that are near the Hopf bifurcation in the stable limit cycle regime. The system settles down to roughly “harmonic” oscillatory behavior whose (nearly) linear appearance is consistent with its proximity to the Hopf bifurcation.

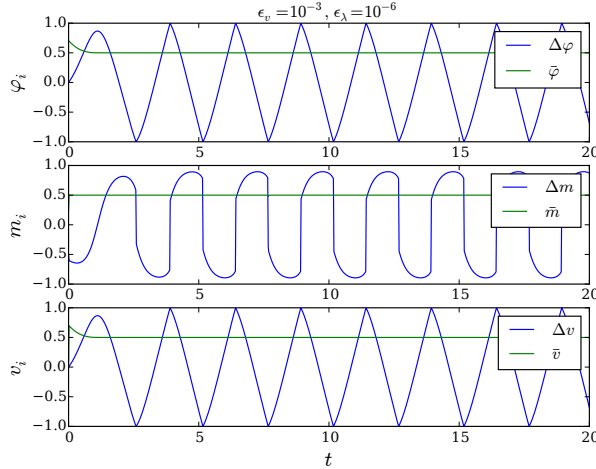


FIG. 5. Both parameters ϵ_v , and ϵ_λ taken to be small, represented by $\epsilon_v = 10^{-3}, \epsilon_\lambda = 10^{-6}$. The system displays oscillatory behavior that is suggestive of a relaxation oscillation. The φ variables are tightly coupled to the v variables due to the small value of ϵ_λ in Equations (17) and (18). The difference variables $\Delta\varphi, \Delta v$ undergo oscillations with sharp transitions, while Δm oscillates in a nonlinear manner. Also note that the mean variables $\bar{\varphi}, \bar{m}$, and \bar{v} appear to stably converge to a value of 0.5: this, combined with the coupling between $\Delta\varphi$ and Δv , strongly suggests that the dynamics can be reduced to a two-dimensional system.

4.1. Dynamics in the limit $\epsilon_\lambda \rightarrow 0$. The limit dynamics (19) inherits the deadlock equilibrium $z_{rd} := h^\dagger(z_d)$ from the full dynamics (12), where

$$(22) \quad z_{rd} := h^\dagger(z_d) = (\Delta\varphi_{rd}, \bar{\varphi}_{rd}, \Delta m_{rd}, \bar{m}_{rd}),$$

$\bar{\varphi}_{rd} = 1/2, \Delta\varphi_{rd} = \Delta m_{rd} = 0$, and \bar{m}_{rd} again solves Equation (20).

In Figure 6 we show the numerically-computed bifurcation diagram for the system (19) with bifurcation parameter ϵ_v . For large values of ϵ_v , the deadlock equilibrium is stable. As ϵ_v is lowered below the critical value $\epsilon_{v,0}$, the system undergoes a Hopf bifurcation that results in a limit cycle. In Figure 6, we plot the amplitude of the oscillations of $\Delta\varphi$ for the limit cycle. As can be seen from Equation (11), $\Delta\varphi$ is constrained to take values in $[-1, 1]$, so the limit cycle's amplitude is bounded above by 1.

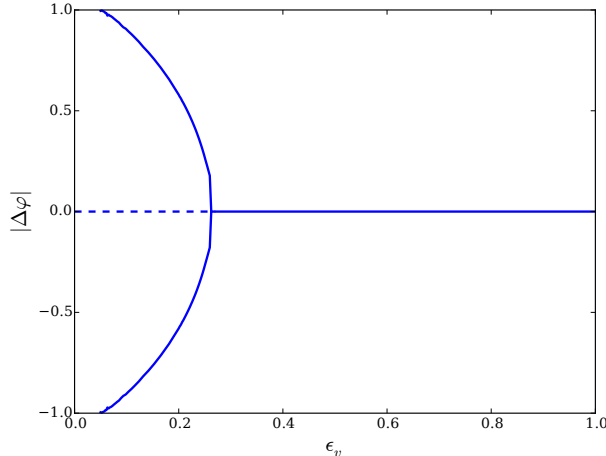


FIG. 6. The numerically-computed bifurcation diagram for the system (19) with $\epsilon_\lambda \rightarrow 0$ and bifurcation parameter ϵ_v . The amplitude of the limit cycle is computed as the amplitude of the oscillations in $\Delta\varphi$. We clearly see a supercritical Hopf bifurcation, with bifurcation value $\epsilon_{v,0}$. The free parameters were set to $c = 1, \sigma = 4$.

4.2. Analysis of the $\epsilon_\lambda \rightarrow 0$ dynamics. Inspired by the bifurcation diagram, we now seek to show the existence of the Hopf bifurcation suggested by Figure 6. The following theorem from [8] summarizes the conditions under which a system undergoes Hopf bifurcation.

THEOREM 3 (Hopf bifurcation, [8, Theorem 3.4.2]). *Suppose that the system $\dot{z} = f(z, \mu), z \in \mathbb{R}^n, \mu \in \mathbb{R}$, has an equilibrium (z_0, μ_0) and the following properties are satisfied:*

1. *The Jacobian $D_z f|_{(z_0, \mu_0)}$ has a simple pair of pure imaginary eigenvalues $\lambda(\mu_0)$ and $\bar{\lambda}(\mu_0)$ and no other eigenvalues with zero real parts,*
2. *$d(\text{Re } \lambda(\mu))/d\mu|_{\mu=\mu_0} = d \neq 0$.*

Property 1) implies that there is a smooth curve of equilibria $(z(\mu), \mu)$ with $z(\mu_0) = z_0$. The eigenvalues $\lambda(\mu), \bar{\lambda}(\mu)$ of $D_z f|_{(z(\mu), \mu)}$ which are imaginary at $\mu = \mu_0$ vary smoothly with μ .

If Property 2) is satisfied, then there is a unique three-dimensional center manifold passing through (z_0, μ_0) in $\mathbb{R}^n \times \mathbb{R}$ and a smooth system of coordinates (preserving the planes $\mu = \text{const.}$) for which the Taylor expansion of degree 3 on the center manifold is given by [8, (3.4.8)]. If $\ell_1|_{(z_0, \mu_0)} \neq 0$, there is a surface of periodic solutions in the center manifold which has quadratic tangency with the eigenspace of $\lambda(\mu_0), \bar{\lambda}(\mu_0)$ agreeing to second order with the paraboloid $\mu = -(\ell_1|_{(z_0, \mu_0)}/d)(x^2 + y^2)$. If $\ell_1|_{(z_0, \mu_0)} < 0$, then these periodic solutions are stable limit cycles, while if $\ell_1|_{(z_0, \mu_0)} > 0$, the periodic

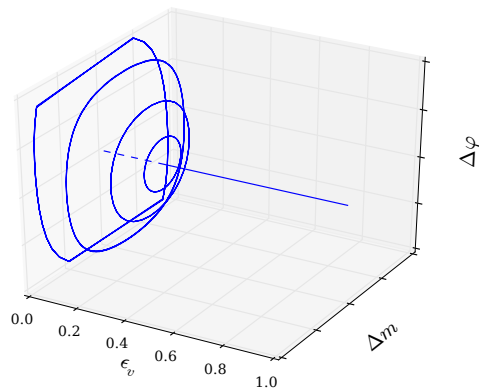


FIG. 7. The numerically-computed bifurcation diagram for the system (19) with $\epsilon_\lambda \rightarrow 0$ and bifurcation parameter ϵ_v . The x-axis is the bifurcation parameter ϵ_v , while the y and z-axes are Δm and $\Delta\varphi$, respectively. As the bifurcation parameter is lowered below $\epsilon_{v,0}$, the deadlock equilibrium becomes unstable and gives birth to a limit cycle which approaches the boundary of the space $(\Delta m, \Delta\varphi) \in [-1, 1]^2$ as $\epsilon_v \rightarrow 0$. The free parameters were set to $c = 1, \sigma = 4$.

solutions are repelling.

The formulae for $\ell_1|_{(z_0, \mu_0)}$, the first Lyapunov coefficient, are given in Appendix A.

REMARK 4. In the statement of Theorem 3 we used μ as the bifurcation parameter for consistency with the notation of [8]. In the analysis in this paper, ϵ_v plays the role of bifurcation parameter.

The Hopf bifurcation theorem applies to our system, as summarized in Theorem 1 stated in Section 2.3.2 and repeated below.

THEOREM 1. The system $\dot{z}_r = f_r(z_r, \epsilon_v)$ defined by (19) has a deadlock equilibrium z_{rd} given by (22). For sufficiently small $\eta > 0$, the dynamics undergo a Hopf bifurcation resulting in stable periodic solutions at $(z_{rd}, \epsilon_{v,0}(\eta))$, where $\eta \ll 1$ is the saturation constant. In the limit $\eta \rightarrow 0$, $\epsilon_{v,0}(0) \approx 0.262$ is the smaller of the two real-valued solutions of $(1 - 4\epsilon_v^2)^2 - 2\epsilon_v = 0$.

Proof of Theorem 1. Let $\epsilon_{v,0} \approx 0.262$ be the smaller of the two real-valued solutions of $(1 - 4\epsilon_v^2)^2 - 2\epsilon_v = 0$. By Lemma 5, in the limit $\eta \rightarrow 0$, the Jacobian J_0 of the system $\dot{z}_r = f(z_r, \epsilon_v)$ evaluated at the deadlock equilibrium $z_{rd}(\epsilon_v)$ has a simple pair of pure imaginary eigenvalues when $\epsilon_v = \epsilon_{v,0}$ that are shown to persist for sufficiently small $\eta > 0$ as well. Therefore, the first condition of the Hopf bifurcation theorem is satisfied for all sufficiently small $0 < \eta \ll 1$.

Lemma 6 establishes that $d(\text{Re } \lambda(\epsilon_v))/d\epsilon_v|_{\epsilon_{v,0}} \neq 0$ for sufficiently small η so the second condition of the Hopf bifurcation theorem is satisfied for $0 < \eta \ll 1$. The result then follows: the system (19) undergoes a Hopf bifurcation as the parameter ϵ_v is lowered through its critical value $\epsilon_{v,0}(\eta)$.

The first Lyapunov coefficient $\ell_1|_{(z_{rd}, \epsilon_{v,0})}$ is negative, as summarized by Lemma 7. This implies that the resulting limit cycles are stable. \square

The following two lemmas, corresponding to the two properties required by Theorem 3, contain the detailed arguments behind the proof of Theorem 1.

LEMMA 5. Let $J_0 := D_{z_r} f_r(z_{rd}, \epsilon_v)$ be the Jacobian of the system $\dot{z}_r = f_r(z_r, \epsilon_v)$ defined by (19) evaluated at the deadlock equilibrium z_{rd} given by (22), considered as a function of ϵ_v . Then, for sufficiently small $\eta > 0$, J_0 has a simple pair of two pure imaginary eigenvalues $\lambda(\epsilon_v)$ and $\bar{\lambda}(\epsilon_v)$ when $\epsilon_v = \epsilon_{v,0}(\eta)$. In the limit $\eta \rightarrow 0$, $\epsilon_{v,0}(0)$ is the smaller of the two real-valued solutions of $(1 - 4\epsilon_v^2)^2 - 2\epsilon_v = 0$.

Proof. The characteristic polynomial of J_0 is computed in (45) in Appendix B.1 and can be expressed as

$$p_4(\lambda) = |J_0 - \lambda I| = (\lambda - j_{22})(\lambda - j_{44})p_2(\lambda),$$

where the final factor is given by coefficients arising directly from specific entries of the (sparse) Jacobian as

$$p_2(\lambda) = \lambda^2 - (j_{11} + j_{33})\lambda + j_{11}j_{33} - j_{13}j_{31}$$

and the components j_{kl} of the Jacobian are as given in Equations (38)–(44) of Appendix B.1.

The roots of p_4 are given by

$$\{j_{22} = -8\bar{m}_{rd}/\sqrt{1+4\eta^2}, j_{44} = -2(\epsilon_v + 4\bar{m}_{rd}) - (1 + 4\bar{m}_{rd})/(2\epsilon_v)\} \cup \{\lambda | p_2(\lambda) = 0\}.$$

It is clear that the first two roots are negative for all $\epsilon_v > 0$, so the stability properties of the deadlock equilibrium are determined by the roots of p_2 .

The roots λ_{\pm} of p_2 are purely imaginary if $j_{11} + j_{33} = 0$. The condition $j_{11} + j_{33} = 0$ implies

$$(23) \quad \bar{m}_{rd} = \frac{1 - 4\epsilon_v^2}{2 + 32\eta^2\epsilon_v/(1 + \eta^2)^{3/2}}.$$

Inserting this expression into the expression (20) for $\bar{m}_d(\epsilon_v)$, one finds that $j_{11} + j_{33} = 0$ implies that

$$(24) \quad \frac{2}{(16\eta^2\epsilon_v + (1 + \eta^2)^{3/2})^2} \left(8\epsilon_v^2(1 + \eta^2)^3 + 2\epsilon_v(1 + 3\eta^2 + 67\eta^4 + \eta^6) - (1 + \eta^2)(1 + \eta^4 + \eta^2(2 - 12\sqrt{1 + \eta^2})) - 16\epsilon_v^4(1 + \eta^2)(1 + \eta^4 + \eta^2(2 - 4\sqrt{1 + \eta^2})) \right) = 0.$$

Discarding the leading term, which is positive for all $\eta \geq 0$, (24) can be written as

$$g_1(\epsilon_v, \eta) = 0.$$

In the limit $\eta \rightarrow 0$, (24) reduces to

$$(25) \quad g_1(\epsilon_v, 0) = (1 - 4\epsilon_v^2)^2 - 2\epsilon_v = 0.$$

This equation has two real-valued solutions, of which only the smaller one, $\epsilon_v = \epsilon_{v,0} \approx 0.262$, also solves $j_{33} = 0$. Therefore the smaller solution is the relevant one defining the bifurcation value.

The derivative $\partial g_1 / \partial \epsilon_v(\epsilon_{v,0}, 0) = -64\epsilon_{v,0}^3 + 16\epsilon_{v,0} + 2 \approx 5.04 > 0$, so the implicit function theorem implies that there exists a continuously differentiable family of solutions $\epsilon_{v,0}(\eta)$ of $g_1(\epsilon_v, \eta) = 0$ such that $\epsilon_{v,0}(0) = \epsilon_{v,0} \approx 0.262$. \square

LEMMA 6. Let $\lambda(\epsilon_v)$ and $\bar{\lambda}(\epsilon_v)$ be the simple pair of pure imaginary eigenvalues and let $\epsilon_{v,0}(\eta)$ be as defined in Lemma 5. Then, for sufficiently small $\eta > 0$, $d(\operatorname{Re} \lambda(\epsilon_v))/d\epsilon_v|_{\epsilon_{v,0}(\eta)} < 0$.

Proof. Let $\epsilon_{v,0}$ and $p_2(\lambda) = \lambda^2 - (j_{11} + j_{33})\lambda + j_{11}j_{33} - j_{13}j_{31}$ be defined as in the proof of Lemma 5, where j_{kl} are defined in Appendix B.1. Let $\Delta_p = (j_{11} + j_{33})^2 - 4(j_{11}j_{33} - j_{13}j_{31})$ be the discriminant of p_2 with respect to λ .

At the bifurcation value $\epsilon_{v,0}$, $j_{11} + j_{33} = 0$, so the discriminant $\Delta_p = -4(j_{11}j_{33} - j_{13}j_{31})$, which is negative, as can be shown by substituting in the expressions for j_{kl} and grouping terms. This implies that the real part of the roots λ_{\pm} are given by $(j_{11} + j_{33})/2$. Therefore, since the coefficients of p_2 are continuous functions of ϵ_v , the sign of the derivative $d(\operatorname{Re} \lambda(\epsilon_v))/d\epsilon_v|_{\epsilon_v=\epsilon_{v,0}}$ is given by that of $(j'_{11} + j'_{33})(\epsilon_{v,0}) := d(j_{11} + j_{33})/d\epsilon_v|_{\epsilon_v=\epsilon_{v,0}}$. Computing the derivative, we get

$$\begin{aligned} (j'_{11} + j'_{33})|_{\epsilon_v=\epsilon_{v,0}} &= g_2(\epsilon_v, \eta) := -\frac{16\eta^2 \bar{m}'_{rd}}{(1 + 4\eta^2)^{3/2}} - 2 - \frac{1 - 2\bar{m}_{rd}}{2\epsilon_v^2} - \frac{\bar{m}'_{rd}}{\epsilon_v} \Big|_{\epsilon_v=\epsilon_{v,0}} \\ &= -2 - \frac{2(1 + \eta^2)^{3/2} + 8\eta^2/\epsilon_v}{(1 + \eta^2)^{3/2} + 16\epsilon_v\eta^2} - \bar{m}'_{rd} \left(\frac{16\eta^2}{(1 + 4\eta^2)^{3/2}} + \frac{1}{\epsilon_v} \right) \Big|_{\epsilon_v=\epsilon_{v,0}}, \end{aligned}$$

where \bar{m}'_{rd} represents the derivative with respect to ϵ_v of the solution (21) and we have used the value of \bar{m}_{rd} from (23) that holds at the bifurcation value.

The series expansion of $g_2(\epsilon_v, \eta)$ in the neighborhood of $(\epsilon_v, \eta) = (\epsilon_{v,0}, 0)$ is

$$g_2(\epsilon_v, \eta) = -4 - \frac{\bar{m}'_{rd}}{\epsilon_v} + \frac{\partial g_2(\epsilon_{v,0}, 0)}{\partial \epsilon_v} (\epsilon_v - \epsilon_{v,0}) + \mathcal{O}(\epsilon_v^2, \eta^2),$$

where $\partial g_2(\epsilon_{v,0}, 0)/\partial \epsilon_v = (1 - 2\bar{m}_{rd})/\epsilon_{v,0}^3 + 2\bar{m}'_{rd}/\epsilon_{v,0}^2 + \bar{m}''_{rd}/\epsilon_{v,0}$ and $\mathcal{O}(\epsilon_v^2, \eta^2)$ represents second order and higher terms in ϵ_v and η . By the argument at the end of the proof of Lemma 5, $\epsilon_{v,0}(\eta)$ is a continuously-differentiable function of η such that $\epsilon_{v,0}(0) = \epsilon_{v,0}$. It is clear that g_2 is analytic for all $\epsilon_v, \eta > 0$, so for small $\eta > 0$, the sign of $g_2(\epsilon_v, \eta)$ is dominated by the sign of the constant (in η) term $-4 - \bar{m}'_{rd}/\epsilon_v$ and we proceed by studying it.

Consider Equation (21) defining $\bar{m}_{rd}(\epsilon_v)$ and define $\Delta = (1 + 4\epsilon_v^2)^2 + 8(1 + 4\epsilon_v)$ as the discriminant of (20) which appears under the radical in (21). Direct computation shows that

$$\bar{m}'_{rd} = \frac{-20 - 56\epsilon_v + 32\epsilon_v^3 + 64\epsilon_v^4}{4\sqrt{\Delta}(1 + 4\epsilon_v)^2} + \frac{\sqrt{\Delta}(4 - 8\epsilon_v - 16\epsilon_v^2)}{4\sqrt{\Delta}(1 + 4\epsilon_v)^2}$$

so that $j'_{33}(\epsilon_v) = -4 - \bar{m}'_{rd}/\epsilon_v$ is equal to

$$(26) \quad \frac{1}{\epsilon_v \sqrt{\Delta}(1 + 4\epsilon_v)^2} \left(n_1(\epsilon_v) - \sqrt{\Delta} n_2(\epsilon_v) \right),$$

where n_1 and n_2 are the polynomials

$$n_1(\chi) := 5 + 14\chi - 8\chi^3 - 16\chi^4; \quad n_2(\chi) := 1 + 2\chi + 28\chi^2 + 64\chi^3.$$

The denominator is strictly positive, so it suffices to check the numerator of (26).

The following argument shows that the numerator is negative, i.e., $n_1(\epsilon_{v,0}) - \sqrt{\Delta(\epsilon_{v,0})} n_2(\epsilon_{v,0}) < 0$. This holds if

$$n_1(\epsilon_{v,0}) < \sqrt{\Delta(\epsilon_{v,0})} n_2(\epsilon_{v,0}).$$

It is clear that $\sqrt{\Delta(\epsilon_{v,0})} > 4$ and that $n_2(\epsilon_{v,0}) > 0$, so it suffices to show that

$$n_1(\epsilon_{v,0}) < 4n_2(\epsilon_{v,0}),$$

which is equivalent to (using the relation $(1 - 4\epsilon_{v,0}^2)^2 - 2\epsilon_{v,0} = 0$ from (25) that holds at the bifurcation point)

$$6 + 12\epsilon_{v,0} - 8\epsilon_{v,0}^2 - 8\epsilon_{v,0}^3 < 4(1 + 2\epsilon_{v,0} + 28\epsilon_{v,0}^2 + 64\epsilon_{v,0}^3)$$

which holds if

$$2 + 4\epsilon_{v,0} - 120\epsilon_{v,0}^2 - 264\epsilon_{v,0}^3 = 2(1 + 2\epsilon_{v,0} - 60\epsilon_{v,0}^2 - 132\epsilon_{v,0}^3) < 0.$$

This last inequality clearly holds at the bifurcation value $\epsilon_{v,0} \approx 0.262$ since $\epsilon_{v,0} > 0.2$ implies that $1 + 2\epsilon_{v,0} - 60\epsilon_{v,0}^2 < 0$.

Thus, the numerator of (26) is strictly negative and therefore $g_2(\epsilon_{v,0}, 0) \neq 0$. By the series expansion argument, this also holds in a neighborhood of $\eta = 0$. This implies that the derivative $d(\operatorname{Re} \lambda(\epsilon_v))/d\epsilon_v|_{\epsilon_v=\epsilon_{v,0}} \neq 0$ for sufficiently small $\eta > 0$. \square

LEMMA 7. *Let $\ell_1 = \ell_1|_{(z_0, \epsilon_0)}$ be the first Lyapunov coefficient of the dynamics (19) evaluated at the deadlock equilibrium z_{rd} given by (22). Then $\ell_1|_{(z_0, \epsilon_0)} < 0$.*

Proof. See Appendix B.2. \square

Theorem 1 then follows as a consequence of Lemmas 5, 6, and 7.

The implication of Theorem 1 is that the system (19) resulting from the limit $\epsilon_\lambda \rightarrow 0$ has a Hopf bifurcation at $\epsilon_v^*(0) = \epsilon_{v,0} \approx 0.262$. However, as can be seen in Figure 4, limit cycle behavior persists for finite ϵ_λ . One can numerically compute the eigenvalues of the linearization of the system (12) evaluated at the deadlock equilibrium z_d and numerically show that a Hopf bifurcation occurs at a value $\epsilon_v^*(\epsilon_\lambda)$. Figure 1 shows the numerically-computed values of $\epsilon_v^*(\epsilon_\lambda)$ for a range of values of ϵ_λ . It is clear that the numerical value for the limit $\lim_{\epsilon_\lambda \rightarrow 0} \epsilon_v^*(\epsilon_\lambda)$ coincides with the analytical value $\epsilon_{v,0}$.

5. Reduction to a planar limit cycle in the joint limit $\epsilon_\lambda, \epsilon_v \rightarrow 0$. The results from Section 4 strongly suggest the existence of a stable limit cycle for finite $\epsilon_v, \epsilon_\lambda$. In this and the following section we make this conclusion rigorous by performing a series of reductions collapsing the dynamics (12) to a planar system in the joint limit $\epsilon_\lambda \rightarrow 0, \epsilon_v \rightarrow 0$. A Poincaré-Bendixson argument affords the conclusion that the planar system exhibits a stable limit cycle. Then, in the next section, we show that this limit cycle persists for small but finite ϵ by applying results from geometric singular perturbation theory.

5.1. A four dimensional attracting invariant submanifold. In our first reduction, we note that $\bar{\varphi}$ and \bar{v} must asymptotically converge to $c/2$ independent of the other states' behavior. This observation reveals an attracting invariant submanifold of dimension four whose restriction dynamics we then study.

We begin by considering the dynamics of $\bar{\varphi}$ independently of the other five dynamical variables, which gives us a nonautonomous system $\dot{\bar{\varphi}} = f_{\bar{\varphi}}(t, \bar{\varphi})$. The following results from [16] concern the asymptotic behavior of a nonautonomous system

$$(27) \quad \dot{x} = f(t, x)$$

defined on $G \subseteq \mathbb{R}^n$. Let G^* be an open set of \mathbb{R}^n containing \bar{G} , the closure of G . We assume that $f : [0, \infty) \times G^* \rightarrow \mathbb{R}^n$ is a continuous (nonautonomous) vector field.

DEFINITION 8. Let $V : [0, \infty) \times G^* \rightarrow \mathbb{R}$ be a continuous, locally Lipschitz function. The function V is said to be a Lyapunov function of (27) on G if

- i. given x in \bar{G} there is a neighborhood N of x such that $V(t, x)$ is bounded from below for all $t \geq 0$ and all x in $N \cap G$.
- ii. $\dot{V}(t, x) \leq -W(x) \leq 0$ for all $t \geq 0$ and all x in G , where W is continuous on \bar{G} . For t where $V(t, x(t))$ is not differentiable, \dot{V} is defined using the right-hand limit.

If V is a Lyapunov function for (27) on G , we define

$$E = \{x; W(x) = 0, x \in \bar{G}\} \text{ and } E_\infty = E \cup \{\infty\}.$$

DEFINITION 9 ([23, Section 6.4]). A real-valued function f on a closed, bounded interval $[a, b]$ is said to be absolutely continuous on $[a, b]$ provided for each $\epsilon > 0$, there is a $\delta > 0$ such that for every finite disjoint collection $\{(a_k, b_k)\}_{k=1}^n$ of open intervals in (a, b) ,

$$\text{if } \sum_{k=1}^n [b_k - a_k] < \delta, \text{ then } \sum_{k=1}^n |f(b_k) - f(a_k)| < \epsilon.$$

Lipschitz continuity implies absolute continuity, as follows:

PROPOSITION 10 ([23, Section 6.4, Proposition 7]). If the function f is Lipschitz on a closed, bounded interval $[a, b]$, then it is absolutely continuous on $[a, b]$.

THEOREM 11 ([16, Theorem 1]). Let V be a Lyapunov function for (27) on G , and let $x(t)$ be a solution of (27) that remains in G for $t \geq t_0 \geq 0$ with $[t_0, \omega)$ the maximal future interval of definition of $x(t)$.

- a. If for each $p \in \bar{G}$ there is a neighborhood N of p such that $|f(t, x)|$ is bounded for all $t \geq 0$ and all x in $N \cap G$, then either $x(t) \rightarrow \infty$ as $t \rightarrow \omega^-$, or $\omega = \infty$ and $x(t) \rightarrow E_\infty$ as $t \rightarrow \infty$.
- b. If $W(x(t))$ is absolutely continuous and its derivative is bounded from above (or from below) almost everywhere on $[t_0, \omega)$ and if $\omega = \infty$, then $x(t) \rightarrow E_\infty$ as $t \rightarrow \infty$.

The following lemma shows that convergence of $\bar{\varphi}$ implies convergence of \bar{v} .

LEMMA 12. If, for the dynamical system (12), $\bar{\varphi}(t) \rightarrow 1/2$ as $t \rightarrow \infty$, then $\bar{v}(t) \rightarrow 1/2$.

Proof. Let $x_1 = \bar{v} - 1/2$ and $u_1 = \bar{\varphi} - 1/2$. Then the dynamics (18) can be written as $\dot{x}_1 = -\lambda(x_1 - u_1)$. It is easily shown that this system is input-to-state stable (ISS) with u_1 as its input. It is a well known result [12, Exercise 4.58] that if the input to an ISS system converges to zero as $t \rightarrow \infty$, then its state converges to zero also. Therefore, $\bar{\varphi}(t) \rightarrow 1/2$ as $t \rightarrow \infty$ implies $\bar{v}(t) \rightarrow 1/2$ as $t \rightarrow \infty$. \square

We now show that $\bar{\varphi}$ converges which, by the preceding lemma, implies the convergence of \bar{v} . For clarity of exposition, we write the argument as a series of lemmas.

LEMMA 13. Let $\epsilon > 0$ and $\mathcal{M} = H_0 \times \Delta^2 \times [0, 1]^2$, and let the set G be defined by

$$G := \{z \in \mathcal{M} | \bar{v} \geq 1/2, \bar{m} > \epsilon\}.$$

The set G is positive invariant under the dynamics $\dot{z} = f_z(z)$ defined by (12).

Proof. Let $z = (\Delta\varphi, \bar{\varphi}, \Delta m, \bar{m}, \Delta v, \bar{v})$ be coordinates for $\mathcal{M} = H_0 \times \Delta^2 \times [0, 1]^2$ and consider the dynamics $\dot{z} = f_z(z)$ defined by (12).

Recall that $\varphi_1(x) = \|x - x_1^*\|$, $\varphi_2(x) = \|x - x_2^*\|$. Writing $(x - x_1^*) + (x_2^* - x) = x_2^* - x_1^*$, the triangle inequality implies that $1 = \|x_2^* - x_1^*\| \leq \|x - x_1^*\| + \|x_2^* - x\| = \varphi_1(x) + \varphi_2(x)$. Therefore $\bar{\varphi} = (\varphi_1(x) + \varphi_2(x))/2 \geq 1/2$.

Furthermore, recall from (18) that $\dot{v} = -\lambda(\bar{v} - \bar{\varphi})$, so $\dot{v}(\bar{v} = 1/2) = -\lambda(1/2 - \bar{\varphi}) \geq 0$ by the lower bound on $\bar{\varphi}$. Therefore the set $\{z \in \mathcal{M} | \bar{v} \geq 1/2\}$ is positive invariant.

Similarly, note that $\bar{m} \geq 0$ by definition and that $-2\bar{m} \leq \Delta m \leq 2\bar{m}$, so $\bar{m} = 0$ implies that $\Delta m = 0$. Therefore, from (16), $\dot{m}(\bar{m} = 0) = \bar{v}/\epsilon_v$, so $\bar{v} \geq 1/2$ implies that $\dot{m}(\bar{m} = 0) \geq c/2\epsilon_v$ and therefore that $\bar{m} > 0$. Therefore, the continuity of the \dot{m} dynamics implies that for $\bar{v} > 1/2$, there exists an $\varepsilon > 0$ such that $\bar{m} < \varepsilon$ implies that $\dot{m}(\bar{m}) > 0$. This implies that G is a positive-invariant set. \square

LEMMA 14. Let $\dot{\bar{\varphi}}$ be defined by (14), which can be written as

$$(28) \quad \dot{\bar{\varphi}} = f_{\bar{\varphi}}(t, \bar{\varphi}) = -\alpha(t)(\bar{\varphi}^2 - (1/2)^2),$$

where the leading coefficient is

$$(29) \quad \alpha(t) := \frac{n(t)}{d(t)} = \frac{m_1\varphi_1|\varphi_1|_\eta + m_2\varphi_2|\varphi_2|_\eta}{\varphi_1\varphi_2|\varphi_1|_\eta|\varphi_2|_\eta}.$$

Then $\alpha(t) \geq 0$ and $\bar{\varphi}(t) \leq \bar{\varphi}(0)$ for any $t > 0$.

Proof. Write the dynamics (14) in the form (28). We proceed by showing that $n(t)$ and $d(t)$ in the definition of $\alpha(t)$ are non-negative.

Note that m_1, m_2, φ_1 , and φ_2 are all non-negative by definition. Now, consider $n(t) = m_1\varphi_1|\varphi_1|_\eta + m_2\varphi_2|\varphi_2|_\eta$. Each term is non-negative by definition, so $n(t) \geq 0$. Similarly, $d(t) = \varphi_1\varphi_2|\varphi_1|_\eta|\varphi_2|_\eta \geq 0$ since it is the product of non-negative terms.

Therefore, $\alpha(t) \geq 0$, since it is the ratio of two non-negative numbers. The quantity $(\bar{\varphi}^2 - (1/2)^2) \geq 0$ since $\bar{\varphi} \geq 1/2$. Thus, $\dot{\bar{\varphi}} \leq 0$, which implies that $\bar{\varphi}(t) \leq \bar{\varphi}(0)$ for any $t > 0$. \square

LEMMA 15. On G , the following lower bound holds:

$$\alpha(t) > \frac{2\eta\varepsilon}{\bar{\varphi}(0)(4\bar{\varphi}(0)^2 + \eta^2)} > 0,$$

where $\alpha(t)$ is defined in (29).

Proof. Recall from the proof of Lemma 14 that $\alpha(t) = n(t)/d(t)$. We proceed by developing a lower bound on $n(t)$ and an upper bound on $d(t)$.

Note that the fact that $m_i > 0$ for $i = 1, 2$ and the definitions of \bar{m} and Δm imply that $-2\bar{m} \leq \Delta m \leq 2\bar{m}$. Consider $n(t)$ and recall that $|\varphi_i|_\eta \geq \eta$ for $i = 1, 2$. The following series of inequalities holds

$$\begin{aligned} n(t) &\geq m_1\varphi_1\eta + m_2\varphi_2\eta \\ &= \frac{\eta}{2}((m_1 + m_2)(\varphi_1 + \varphi_2) + (m_1 - m_2)(\varphi_1 - \varphi_2)) = \frac{\eta}{2}(4\bar{m}\bar{\varphi} + \Delta m\Delta\varphi) \\ &\geq 2\eta\bar{m}(2\bar{\varphi} - \Delta\varphi) \geq 2\eta\varepsilon(2\bar{\varphi} - \Delta\varphi) =: \underline{n}(t), \end{aligned}$$

where the second inequality follows from the fact that $\Delta m \geq -2\bar{m}$ and the third from the fact that $\bar{m} > \varepsilon$ on G .

Now we turn to $d(t)$. Note that $\varphi_1, \varphi_2 \geq 0$ implies that $\varphi_1(t), \varphi_2(t) \leq 2\bar{\varphi}(t) \leq$

$2\bar{\varphi}(0)$. Then the following series of inequalities holds

$$\begin{aligned} d(t) &\leq \varphi_1 \varphi_2 |2\bar{\varphi}(0)|_\eta^2 = \varphi_1 \varphi_2 \sqrt{4\bar{\varphi}(0)^2 + \eta^2} \sqrt{4\bar{\varphi}(0)^2 + \eta^2} \\ &\leq (2\bar{\varphi}(0)) \frac{2\bar{\varphi} - \Delta\varphi}{2} (4\bar{\varphi}(0)^2 + \eta^2) \\ &= \bar{\varphi}(0)(2\bar{\varphi} - \Delta\varphi)(4\bar{\varphi}(0)^2 + \eta^2) =: \bar{d}(t). \end{aligned}$$

A lower bound on $\alpha(t)$ can then be stated as

$$\alpha(t) > \frac{\underline{n}(t)}{\bar{d}(t)} = \frac{2\eta\varepsilon(2\bar{\varphi} - \Delta\varphi)}{\bar{\varphi}(0)(2\bar{\varphi} - \Delta\varphi)(4\bar{\varphi}(0)^2 + \eta^2)} = \frac{2\eta\varepsilon}{\bar{\varphi}(0)(4\bar{\varphi}(0)^2 + \eta^2)},$$

which is clearly positive. \square

Let $W(\bar{\varphi}) = \eta\varepsilon(\bar{\varphi} - 1/2)^2 / (\bar{\varphi}(0)(4\bar{\varphi}(0)^2 + \eta^2))$. Then the following holds.

LEMMA 16. *The function $V = \frac{1}{2}(\bar{\varphi} - 1/2)^2$ is a Lyapunov function of $\dot{\bar{\varphi}} = f_{\bar{\varphi}}(t, \bar{\varphi})$ obeying $\dot{V} \leq -W(\bar{\varphi})$. The function $W(\bar{\varphi})$ takes its unique zero at $\bar{\varphi} = 1/2$.*

Proof. Let $V(\bar{\varphi}, t) = \frac{1}{2}(\bar{\varphi} - (1/2))^2$. Note that $V \geq 0$, so it satisfies condition i of Definition 8. Computing \dot{V} , we find

$$\begin{aligned} \dot{V} &= \partial V / \partial \bar{\varphi} \dot{\bar{\varphi}} = -\alpha(t)(\bar{\varphi}^2 - (1/2)^2)(\bar{\varphi} - (1/2)) \\ &= -\alpha(t)(\bar{\varphi} - 1/2)^2(\bar{\varphi} + 1/2) \\ &\leq -2\eta\varepsilon(\bar{\varphi} - 1/2)^2(\bar{\varphi} + 1/2) / (\bar{\varphi}(0)(4\bar{\varphi}(0)^2 + \eta^2)) \\ &\leq -2\eta\varepsilon(\bar{\varphi} - 1/2)^2 / (\bar{\varphi}(0)(4\bar{\varphi}(0)^2 + \eta^2)) =: -W(\bar{\varphi}), \end{aligned}$$

where the first inequality derives from Lemma 15 and the second from the bound $\bar{\varphi} \geq 1/2$. Therefore condition ii of Definition 8 is satisfied and V is a Lyapunov function for $f_{\bar{\varphi}}$.

It is clear that $W(\bar{\varphi}) \geq 0$, with equality only if $\bar{\varphi} = 1/2$. \square

LEMMA 17. *The function $W(\bar{\varphi}(t))$ is absolutely continuous in t .*

Proof. Proposition 10 shows that Lipschitz continuity implies absolute continuity. It is well known that a function is Lipschitz continuous if it has bounded first derivative, so we proceed by bounding the derivative $dW(\bar{\varphi}(t))/dt$. We require the following bounds on parts of the derivative.

Define $s_{\pm} = |2\bar{\varphi} \pm \Delta\varphi|_{2\eta}$ and rewrite $\alpha(t)$ as $\tilde{n}(t)/\tilde{d}(t)$, where the factors \tilde{n} and \tilde{d} are defined as $\tilde{n}(t) = 2((2\bar{m} + \Delta m)(2\bar{\varphi} + \Delta\varphi)s_{+} + (2\bar{m} - \Delta m)(2\bar{\varphi} - \Delta\varphi)s_{-})$ and $\tilde{d}(t) = (4\bar{\varphi}^2 - \Delta\varphi^2)s_{+}s_{-}$. Finally, rewrite $d(t)$ as $\tilde{d}(t) = ((4\bar{\varphi}^2 - \Delta\varphi^2)/4)|\varphi_1|_{\eta}|\varphi_2|_{\eta}$.

Consider the quantity $(4\bar{\varphi}^2 - 1)/(4\bar{\varphi}^2 - \Delta\varphi^2)$ and recall that $\bar{\varphi} \geq 1/2$. Two applications of the triangle inequality similar to the one in the proof of Lemma 13 show that $-1 \leq \Delta\varphi \leq 1$, which implies that $\Delta\varphi^2 \leq 1$. Taken together, these facts imply that

$$(30) \quad 0 \leq \frac{4\bar{\varphi}^2 - 1}{4\bar{\varphi}^2 - \Delta\varphi^2} \leq 1.$$

Furthermore, recall from the proof of Lemma 15 that $\varphi_i \leq 2\bar{\varphi}(0)$ and that $|\varphi_i|_{\eta} \geq \eta$ for $i = 1, 2$. Taken together, these facts imply the following bounds on φ_i :

$$(31) \quad \eta \leq |\varphi_i|_{\eta} \leq |2\bar{\varphi}(0)|_{\eta}, \quad i = 1, 2.$$

Defining $\beta = \eta\varepsilon/(\bar{\varphi}(0)(4\bar{\varphi}(0)^2 + \eta^2))$, where β is clearly finite, W can be written as $W(\bar{\varphi}) = \beta(\bar{\varphi} - 1/2)^2$. Then the time derivative is

$$\begin{aligned} \frac{dW}{dt} &= \frac{\partial W}{\partial \bar{\varphi}} \dot{\bar{\varphi}} = 2\beta(\bar{\varphi} - 1/2)(-\alpha(t)(\bar{\varphi}^2 - (1/2)^2)) \\ &= -\frac{\beta(\bar{\varphi} - 1/2)n(t)}{|\varphi_1|_\eta|\varphi_2|_\eta} \frac{4\bar{\varphi}^2 - 1}{4\bar{\varphi}^2 - \Delta\varphi^2}. \end{aligned}$$

Then (30) implies that

$$(32) \quad |dW/dt| < \left| \frac{\beta(\bar{\varphi} - 1/2)n(t)}{|\varphi_1|_\eta|\varphi_2|_\eta} \right|.$$

Now we bound the components of (32). The lower bound of (31) implies that $|\varphi_1|_\eta|\varphi_2|_\eta \geq \eta^2$. The upper bound of (31) implies that

$$\begin{aligned} n(t) &= m_1\varphi_1|\varphi_1|_\eta + m_2\varphi_2|\varphi_2|_\eta \\ &\leq (m_1\varphi_1 + m_2\varphi_2)|2\bar{\varphi}(0)|_\eta \\ &\leq 2\bar{\varphi}(0)(m_1 + m_2)|2\bar{\varphi}(0)|_\eta \\ &\leq 2\bar{\varphi}(0)|2\bar{\varphi}(0)|_\eta, \end{aligned}$$

where the second inequality follows from the fact that $\varphi_i \leq 2\bar{\varphi}(0)$, and the third inequality follows from the fact that $m_1 + m_2 \leq 1$ from the definition of the simplex Δ^2 . Finally, Lemma 14 allows us to conclude that $\bar{\varphi} - 1/2 \leq \bar{\varphi}(0) - 1/2$.

Putting together the bounds on the components, we arrive at the bound

$$\begin{aligned} \left| \frac{dW}{dt} \right| &< \frac{\beta(\bar{\varphi}(0) - 1/2)(2\bar{\varphi}(0)|2\bar{\varphi}(0)|_\eta)}{\eta^2} \\ &= \frac{2\varepsilon(\bar{\varphi}(0) - 1/2)}{\eta|2\bar{\varphi}(0)|_\eta}, \end{aligned}$$

which shows that $|dW/dt|$ is finite for all t . This implies that $W(t)$ is Lipschitz on $[0, T]$ for all finite T with Lipschitz constant at most $2\varepsilon(\bar{\varphi}(0) - 1/2)/(\eta|2\bar{\varphi}(0)|_\eta)$. \square

Lemmas 13–17 imply that $\bar{\varphi} \rightarrow 1/2$, which implies that $\bar{v} \rightarrow 1/2$, as formalized in the following lemma.

LEMMA 18. *The variables $\bar{\varphi}$ and \bar{v} asymptotically converge to $1/2$. Therefore, the four-dimensional submanifold \mathcal{M}_4 defined by $\mathcal{M}_4 = \{z = (\Delta\varphi, \bar{\varphi}, \Delta m, \bar{m}, \Delta v, \bar{v}) \in \mathcal{M} | \bar{\varphi} = \bar{v} = 1/2\}$ is an attracting invariant submanifold under the (autonomous) dynamics (12).*

Proof. Lemmas 16 and 17 show that V is a Lyapunov function for the dynamical system $\dot{\bar{\varphi}} = f_{\bar{\varphi}}(\bar{\varphi})$ whose total derivative \dot{V} is upper bounded by $-W(\bar{\varphi})$. Therefore condition b for Theorem 11 holds.

Applying Theorem 11, we get that $\bar{\varphi}$ converges to the unique root of $W(\bar{\varphi})$, which is located at $\bar{\varphi} = 1/2$. Now, applying Lemma 12, we conclude that $\bar{v} \rightarrow 1/2$. Therefore, \mathcal{M}_4 is an attracting set. \square

5.2. A two-dimensional slow manifold in the limit $\epsilon_\lambda \rightarrow 0, \epsilon_v \rightarrow 0$. We now proceed to eliminate Δv and \bar{m} by taking the singular perturbation limit $\epsilon_\lambda \rightarrow 0, \epsilon_v \rightarrow 0$. The first limit couples Δv to $\Delta\varphi$, as in Section 4, while the second limit pushes \bar{m} to a slow manifold $\bar{m}(\Delta\varphi, \Delta m)$. This results in a planar “singular” system.

We study the dynamics (12) restricted to \mathcal{M}_4 defined in Lemma 18 by singular perturbation in the small parameter ϵ_v . Further, let $\ell > 0$ be a positive number such that $\epsilon_\lambda = 1/\lambda = \ell\epsilon_v$. For a given value of ℓ , this links ϵ_λ to ϵ_v . Defining¹ $x = (\Delta\varphi, \Delta m) \in \mathcal{X} := [-1, 1]^2$ and $y = ((1 - 2\bar{m})/\epsilon_v, \Delta v) \in \mathbb{R}_+ \times [-1, 1]$, the restricted dynamics can be written in the standard form for a singular perturbation problem:

$$(33) \quad \dot{x} = f_x(x, y, \epsilon_v)$$

$$(34) \quad \epsilon_v \dot{y} = g_y(x, y, \epsilon_v),$$

where the slow dynamics is given by

$$\begin{aligned} \dot{x}_1 = f_{x,1}(x, y, \epsilon_v) &= \frac{(1 - \epsilon_v y_1 - x_2)(1 - x_1)r_+ - (1 - \epsilon_v y_1 + x_2)(1 + x_1)r_-}{r_+ r_-} \\ \dot{x}_2 = f_{x,2}(x, y, \epsilon_v) &= -\epsilon_v \left(\frac{1 - \epsilon_v y_1 + x_2}{1 + x_1} - \frac{1 - \epsilon_v y_1 - x_2}{1 - x_1} \right) \\ &\quad + \frac{x_2 y_1}{2} + \frac{y_1}{2} (3 - \epsilon_v y_1) x_1, \end{aligned}$$

with $r_\pm = |1 \pm x_1|_{2\eta}$, and the fast dynamics is given by

$$\begin{aligned} \epsilon_v \dot{y}_1 = g_{y,1}(x, y, \epsilon_v) &= \epsilon_v \left(\frac{1 - \epsilon_v y_1 + x_2}{1 + x_1} + \frac{1 - \epsilon_v y_1 - x_2}{1 - x_1} \right) \\ &\quad - \frac{y_1}{2} \left((1 + x_1) \left(1 + \frac{1 - \epsilon_v y_1 + x_2}{2} \right) \right. \\ &\quad \left. + (1 - x_1) \left(1 + \frac{1 - \epsilon_v y_1 - x_2}{2} \right) \right) \\ &\quad + \frac{\sigma}{2} ((1 - \epsilon_v y_1)^2 - x_2^2) \\ \epsilon_v \dot{y}_2 = g_{y,2}(x, y, \epsilon_v) &= -\frac{1}{\ell} (y_2 - x_1). \end{aligned}$$

It can be easily verified that the vector field f_x points inward on the boundary of $\mathcal{X} = [-1, 1]^2$, so \mathcal{X} is positive invariant.

The slow manifold \mathcal{M}_s is given by the implicit function solution $y = h_y(x)$ of the limiting fast dynamics $g(x, h_y(x), 0) = 0$:

$$(35) \quad \begin{aligned} y_1 &= \frac{\sigma(1 - x_1^2)}{3 + x_1 x_2} =: h_{y,1}(x) \\ y_2 &= x_1 =: h_{y,2}(x). \end{aligned}$$

Figure 8 compares the analytically-computed slow manifold $h_{y,1}(x(t))$ to the value of $y_1(t)$ computed based on a numerical simulation of the full six-dimensional system (12). The small value of the error between the two values shows that the low-dimensional slow manifold is a good approximation to the trajectory of the high-dimensional system. Figure 9 shows the analytically-computed slow manifold surface $h_{y,1}(x)$ along with the trajectories $h_{y,1}(x(t))$ and $y_1(t)$. The figure clearly shows the relaxation oscillation structure of the limit cycle, which consists of alternating slow

¹This definition, which we make for consistency with the literature on singular perturbation problems, overloads the definition of $x \in \mathcal{D}$ from Section 2.

and fast segments. The slow segments where $\Delta\varphi$ evolves correspond to the physical dynamics of navigating from the goal x_1^* to x_2^* and vice versa, while the fast segments where Δm jumps correspond to the agent quickly changing its mind and deciding to switch motivations after having achieved its task.

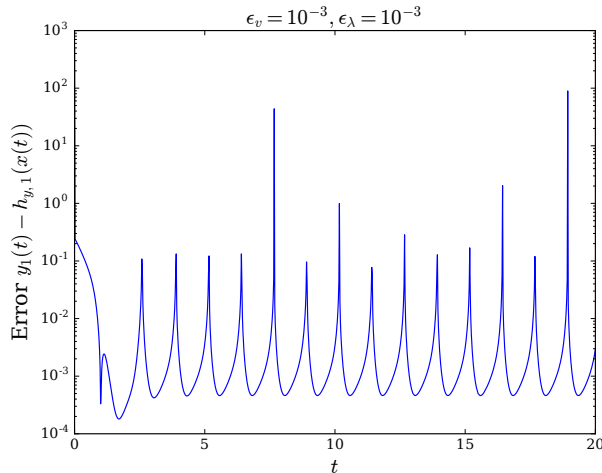


FIG. 8. Error in the slow manifold approximation (35) computed for $\epsilon_v = 10^{-3}$, $\epsilon_\lambda = 10^{-3}$, plotted on a logarithmic scale. The blue trace shows the error $y_1(t) - h_{y,1}(x(t))$ for $y_1(t) = (1 - 2\bar{m}(t))/\epsilon_v$ computed from a simulated trajectory of the full six-dimensional system (12) and $h_{y,1}(x(t))$, the analytical expression for the slow manifold evaluated along the same trajectory. The spikes correspond to the fast transitions between sections of the slow manifold (corresponding to fast jumps of $x_2 = \Delta m$ between $+1$ and -1), which can be clearly seen in Figure 9. The small magnitude of the error shows that the analytical slow manifold is a good approximation to the full system.

The planar reduced dynamics on the slow manifold are given by the restriction of (33) to the slow manifold \mathcal{M}_s , now expressed in the coordinates of $\mathcal{X} = [-1, 1]^2$,

$$(36) \quad \dot{x} = f_x(x, h_y(x), 0),$$

where the components are

$$\begin{aligned} \dot{x}_1 = f_{x,1}(x, h_y(x), 0) &= \frac{(1 - x_1)(1 - x_2)r_+ - (1 + x_1)(1 + x_2)r_-}{r_+ r_-} \\ \dot{x}_2 = f_{x,2}(x, h_y(x), 0) &= \frac{\sigma(1 - x_2^2)(x_2 + 3x_1)}{2(3 + x_1 x_2)}. \end{aligned}$$

As seen in Appendix C, the slow manifold \mathcal{M}_s is hyperbolic if the initial layer equation, (55), $\delta y = D_y g_y(x, 0, 0)\delta y$ (where $\delta y = y - h(x)$) has a hyperbolic equilibrium at the origin. The eigenvalues of the linearization $\left. \frac{\partial g_y}{\partial y} \right|_{(x,0,0)}$ are equal to $-1/\ell$ and $-(3 + x_1 x_2)/2$. The slow variables (x_1, x_2) lie in $\mathcal{X} = [-1, 1]^2$ and $\ell > 0$ by definition, so both eigenvalues are strictly negative. Therefore they never intersect the imaginary axis and the slow manifold \mathcal{M}_s is hyperbolic.

5.3. Existence of a stable limit cycle in the planar system. Now, we study the planar dynamics (36) and show by a straightforward application of the Poincaré-Bendixson Theorem [8, Theorem 1.8.1] that they exhibit an isolated periodic orbit —

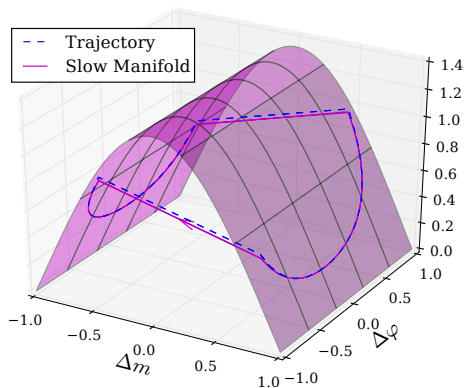


FIG. 9. Orbits on the slow manifold \mathcal{M}_s defined by (35) computed for $\epsilon_v = 10^{-3}, \epsilon_\lambda = 10^{-6}$. The blue trace shows $y_1(t) = (1 - 2\bar{m}(t))/\epsilon_v$ computed from a simulated trajectory of the full six-dimensional system (12), while the magenta trace shows $y_1(t) = h_1(x(t))$, the analytical expression for the slow manifold evaluated along the same trajectory. The shaded surface shows the slow manifold surface $h_1(x)$. The close correspondence between the two traces shows that the analytical slow manifold is a good approximation to the full system. The structure of these orbits (alternation of arcs nearly-embedded in \mathcal{M}_s connected by departing near-line segments) arises from the concatenation of slow evolution corresponding to navigation (and changes in $\Delta\varphi$) and fast jumps corresponding to the agent changing its prioritization (reflected in switching the sign of Δm).

a limit cycle — attracting an open annular neighborhood of the origin. We conjecture (and all numerical evidence corroborates) that this is an asymptotically stable limit cycle comprising the forward limit set of the entire origin-punctured state space. For present purposes it suffices to observe formally that an open neighborhood of initial conditions around the origin must take their forward limit set on this limit cycle.

LEMMA 19. Let $c = 1$. For $\sigma > 48\eta^2/(1 + 4\eta^2)^{3/2}$, there exists a periodic orbit of the reduced system (36) whose basin includes an open annular neighborhood excluding the (unstable) origin.²

Proof. Note that the set $\mathcal{X} = [-1, 1]^2$ is invariant set under the reduced dynamics $\dot{x} = f_x(x, h_y(x), 0)$. Furthermore, note that the only equilibria in \mathcal{X} are the origin and the four corners $(x_1, x_2) = (\pm 1, \pm 1)$. It is easy to see that the boundary of \mathcal{X} is an invariant set; each corner is a saddle, and each edge is a heteroclinic orbit connecting two saddles. Let \mathcal{X}° be the interior of \mathcal{X} . Then \mathcal{X}° is pre-compact, connected, and contains a single fixed point at the origin.

The linearization of the reduced dynamics at the origin is given by

$$J_{r,0} = \frac{1}{\sqrt{1 + 4\eta^2}} \begin{bmatrix} -8\eta^2/(1 + 4\eta^2) & -2 \\ \sigma/2 & \sigma/6 \end{bmatrix}.$$

The determinant $\det J_{r,0} = (\sigma/(1 + 4\eta^2)^{3/2})(1 + 8\eta^2/3) > 0$ for all $\sigma, \eta > 0$ and the trace $\text{tr } J_{r,0} = \sigma/6 - 8\eta^2/(1 + 4\eta^2)^{3/2} > 0$ for all $\sigma > 48\eta^2/(1 + 4\eta^2)^{3/2}$. The trace

²In the limit $\eta \rightarrow 0$, the periodic orbit exists for all $\sigma > 0$, as can be seen by taking the limit of the expression in the Lemma.

and determinant are, respectively, the sum and product of the two eigenvalues, so the fact that they are both positive implies that the eigenvalues are themselves positive. Therefore, for $\sigma > 48\eta^2/(1 + 4\eta^2)^{3/2}$, the origin is an unstable focus. In the limit $\eta \rightarrow 0$, the condition becomes $\sigma > 0$.

Since the entire annular region, $\overset{\circ}{\mathcal{X}} \setminus \{0\}$, is a pre-compact, positive invariant set possessing no fixed points it follows from the Poincaré-Bendixson Theorem that its forward limit set consists of proper (non-zero period) periodic orbits. In particular, in the neighborhood of the excluded repeller at the origin, there must exist an isolated periodic orbit comprising the forward limit set for that entire (punctured) neighborhood. \square

6. Persistence of the limit cycle for finite $\epsilon_v, \epsilon_\lambda$. We now give conditions (which were previously stated as Theorem 2 in Section 2.3.2) under which the limit cycle whose existence was proven in the limit $\epsilon_\lambda \rightarrow 0, \epsilon_v \rightarrow 0$ in Lemma 19 persists for finite values of $\epsilon_\lambda, \epsilon_v$. The result depends upon the conjectured hyperbolicity of that cycle, for which we establish numerical evidence below.

THEOREM 2. *Accepting Conjecture 21, below, for $\sigma = 4$, there exists a stable limit cycle of (12) for sufficiently small, but finite, values of ϵ_λ and ϵ_v . Equivalently, fixing λ , there exists a stable limit cycle of (12) for sufficiently large, but finite, values of v^* .*

Lemma 19 shows that the singularly perturbed system with $\epsilon \rightarrow 0$, i.e., $\epsilon_v, \epsilon_\lambda \rightarrow 0$ exhibits a limit cycle γ_0 . The following result due to Fenichel [6] then allows us to show that this limit cycle persists for sufficiently small $\epsilon_v, \epsilon_\lambda > 0$.

Two pieces of notation are required to state the result. The symbol \mathcal{E}_H represents the open set on which the linearization of the dynamics normal to the slow manifold has hyperbolic fixed points. In \mathcal{E}_H the reduced vector field X_R is defined by

$$X_R(m) = \pi^\mathcal{E} \partial / \partial \epsilon X^\epsilon(m)|_{\epsilon=0},$$

where $\pi^\mathcal{E}$ is the projection onto \mathcal{E} defined in Equation (57) of Appendix C. We can now state the result.

THEOREM 20 ([6, Theorem 13.1]). *Let M be a C^{r+1} manifold, $2 \leq r \leq \infty$. Let $X^\epsilon, \epsilon \in (-\epsilon_0, \epsilon_0)$ be a C^r family of vector fields, and let \mathcal{E} be a C^r submanifold of M consisting entirely of equilibrium points of X^0 . Let $\gamma \in \mathcal{E}_H$ be a periodic orbit of the reduced vector field X_R , and suppose that γ_0 , as a periodic orbit of X_R , has 1 as a Floquet multiplier of multiplicity precisely one. Then there exists $\epsilon_1 > 0$ and there exists a C^{r-1} family of closed curves $\gamma_\epsilon, \epsilon \in (-\epsilon_1, \epsilon_1)$, such that $\gamma_0 = \gamma$ and γ_ϵ is a periodic orbit of $\epsilon^{-1}X^\epsilon$. The period of γ_ϵ is a C^{r-1} function of ϵ .*

Theorem 13.2 of [6] states that, when γ_0 is hyperbolic, the stability of the family γ_ϵ of periodic orbits for $\epsilon > 0$ can be deduced from the stability of γ_0 and the stability of the linearization of f_x, g_y at $\epsilon = 0$.

CONJECTURE 21. *Let $\sigma = 4$. The periodic orbit, γ_0 , whose existence is guaranteed by Lemma 19 for the reduced dynamics $\dot{x} = f_x(x, h_y(x), 0)$ defined by (36) is asymptotically stable with Floquet multipliers $\rho_1 = 1, \rho_2 < 1$.*

The Floquet multiplier associated with perturbations along the vector field is always equal to 1, and the remaining $n - 1$ multipliers are the eigenvalues of the linearized Poincaré map DP of the periodic orbit [8, Section 1.5]. We proceed by computing the numerical approximation to P and DP for the case $\sigma = 4, c = 1$ using the Poincaré section $\Sigma = \{(x_1, 0) | 0.1 < x_1 < 1\}$. The results are shown in Figure

10. From studying numerical solutions of the reduced dynamics, we know that the periodic orbit crosses Σ at a point p near the border at $x_1 = 1$. To five decimal digits, $P(p)$ is constant for $p > 0.45$. This suggests that the linearized map $DP(p)$ has a value less than $10^{-5} < 1$. This implies that the two Floquet multipliers are $\mu_1 = 1, \mu_2 < 10^{-5} < 1$.

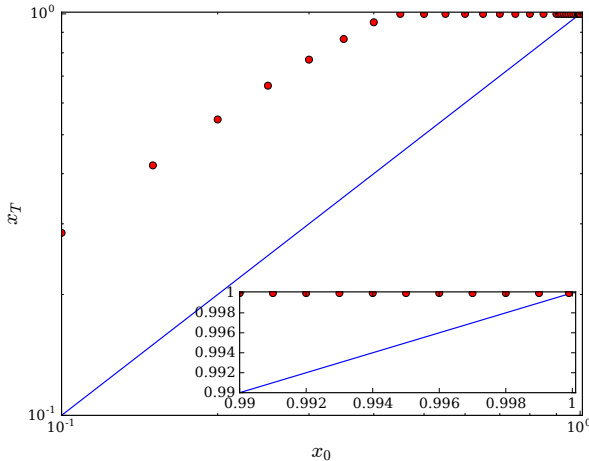


FIG. 10. Poincaré map of (36) computed for the section $\Sigma = \{(x_1, 0) | 0.1 < x_1 < 1\}$, plotted on logarithmic axes. Inset: an enlarged view of the map for the section $0.99 < x_1 < 1$, plotted on linear axes. In both cases, the blue line represents the identity map, so values above the line represent stable behavior.

In Conjecture 21, we only make claims about the Floquet multipliers in the case where σ takes its nominal value $\sigma = 4$. However, numerical investigation suggests that this result holds for generic positive values of σ . Theorem 2 then follows from applying Theorem 20 to the (now conjectured to be stable) limit cycle found in Lemma 19.

Proof of Theorem 2. Let γ be a periodic orbit of the reduced system whose existence is shown in Lemma 19. By Conjecture 21, γ has 1 as a Floquet multiplier of multiplicity precisely 1. The eigenvalues μ_1, μ_2 of the linearization $\partial g_y / \partial y$ can be computed in closed form and take the values

$$\mu_1 = -\frac{1}{\ell}, \quad \mu_2 = -\frac{(3 + x_1 x_2)}{2}.$$

On the slow manifold $(x_1, x_2) \in \mathcal{X} = [-1, 1]^2$ these are bounded away from the imaginary axis, so $\gamma \in \mathcal{E}_H$. Then, by Theorem 20, there exists $\epsilon_1 > 0$ and a family of periodic orbits $\gamma_\epsilon, \epsilon \in (-\epsilon_1, \epsilon_1)$ such that $\gamma_0 = \gamma$.

Specifically, for each $\epsilon \in (0, \epsilon_1)$, there exists a stable limit cycle γ_ϵ with $\epsilon_v = \epsilon$ and $\epsilon_\lambda = \ell\epsilon$. Equivalently, fix $\lambda > 0$ and define $v_1^* = 1/\epsilon_1 < +\infty$. Then for $v^* > v_1^*$, there exists a stable limit cycle γ_ϵ for $\epsilon = \epsilon_v = 1/v^*$. \square

COROLLARY 22. *Theorem 2 establishes the existence of a stable periodic orbit of the reduced dynamics for $(\epsilon_\lambda, \epsilon_v) \in \mathbb{R}_+ \times [0, \epsilon_1)$, i.e., the neighborhood of the ϵ_λ axis for sufficiently small $\epsilon_v > 0$ and generic ϵ_λ .*

Proof. Note that the fast dynamics (34) defines $\epsilon_\lambda = \ell\epsilon_v$, specifying only that $\ell > 0$. Therefore, the result of Theorem 2 applies for parameter values $(\epsilon_\lambda, \epsilon_v) \in$

$\{(\ell\epsilon_v, \epsilon_v) | \epsilon_v \in [0, \epsilon_1], \ell \in \mathbb{R}_+\}$. □

7. Conclusion. In summary, we have developed a dynamical systems method to managing motivations in physically-embodied agents, i.e., robots. This method provides a novel way for a system to autonomously and continuously switch between a set of vector fields, each of which defines a possible dynamics for the physical state of the system that corresponds to performing a navigation task.

We specialize to the case where the system has two vector fields defined on a simply-connected subset of \mathbb{R}^2 . By imposing several symmetries on our system, we are able to analyze the system in the limit where first one, and then both, of two parameters approaches zero. In the joint limit we reduce the system to a planar dynamical system by means of a singular perturbation analysis; a Poincaré-Bendixson argument shows that this planar system exhibits an isolated periodic orbit corresponding to the physical system state oscillating between two fixed points, one for each of the two vector fields. By appealing to geometric singular perturbation theory, we show that this periodic orbit persists for finite values of the two parameters.

A natural extension of this work is to consider cases where the system has more than two navigation tasks and where the domain \mathcal{D} is punctured by obstacles, i.e., not simply connected. One natural way to extend this work to the case of multiple tasks is to decompose tasks into hierarchies encoded in binary trees; then, a variant of the system studied in this paper can run in each node to manage the motivations represented by each of its child nodes. By designing an appropriate method to feed the information from the child nodes back to their parent, it will be possible to maintain the limit cycle behavior for the larger number of tasks. Extending the analysis in this paper to the case of non-simply connected domains may prove more complex, as the analysis relies on several coordinate transformations that will be difficult to extend the more general case.

The other natural extension of this work is to apply it by implementing the motivational system on a physical robot. This implementation work is already in progress and will be the subject of a future report.

Appendix A. First Lyapunov coefficient calculation. Kuznetsov [15, Section 5.4] provides the following formulae for computing $\ell_1|_{(z_0, \epsilon_0)}$, the first Lyapunov coefficient of the dynamics $\dot{z} = f(z, \epsilon)$. Let $J_0 = D_z f|_{(z_0, \epsilon_0)}$. Property 1 of Theorem 3 implies that J_0 has two pure imaginary eigenvalues $\lambda(\epsilon_0), \bar{\lambda}(\epsilon_0) = \pm i\omega_0, \omega_0 > 0$. Let $q \in \mathbb{C}^n$ be a complex eigenvector corresponding to $\lambda(\epsilon_0)$:

$$J_0 q = i\omega_0 q, \quad J_0 \bar{q} = -i\omega_0 \bar{q}.$$

Introduce the adjoint eigenvector $p \in \mathbb{C}^n$ satisfying

$$J_0^T p = -i\omega_0 p, \quad J_0^T \bar{p} = i\omega_0 \bar{p}$$

and satisfying the normalization condition $\langle p, q \rangle = 1$, where $\langle \cdot, \cdot \rangle$ is the standard inner product on \mathbb{C}^n .

Then, Taylor expand $f(z) = f(z, \epsilon_0)$ to third order in z :

$$f(z) = \frac{1}{2}B(z, z) + \frac{1}{6}C(z, z, z) + \mathcal{O}(\|z\|^4),$$

where B and C are multilinear functions given by

$$B_i(x, y) = \sum_{j,k=1}^n \frac{\partial^2 f_i(\xi, \epsilon)}{\partial \xi_j \partial \xi_k} \Big|_{\xi=0} x_j y_k := \sum_{j,k=1}^n B_{ijk} x_j y_k,$$

$$\begin{aligned}
C_i(x, y, z) &= \sum_{j,k,l=1}^n \frac{\partial^3 f_i(\xi, \epsilon)}{\partial \xi_j \partial \xi_k \partial \xi_l} \Big|_{\xi=0} x_j y_k z_l \\
&:= \sum_{j,k,l=1}^n C_{ijkl} x_j y_k z_l,
\end{aligned}$$

which define the coefficients B_{ijk} and C_{ijkl} . The coefficient $\ell_1|_{(z_0, \epsilon_0)}$ is then given by Equation (5.62) of [15]:

$$\begin{aligned}
(37) \quad \ell_1|_{(z_0, \epsilon_0)} &= \frac{1}{2\omega_0} \operatorname{Re} \left[\langle p, C(q, q, \bar{q}) \rangle - 2\langle p, B(q, J_0^{-1}B(q, \bar{q})) \rangle \right. \\
&\quad \left. + \langle p, B(\bar{q}, (2i\omega_0 I - J_0)^{-1}B(q, q)) \rangle \right],
\end{aligned}$$

where I is the identity matrix.

Appendix B. Analysis of the Hopf bifurcation of (19). In this section, we report computations relevant to the results in Theorem 1.

B.1. Jacobian computation. The following claim, which can be verified by direct computation, establishes the value of the Jacobian J_0 of the dynamics (19) evaluated at the deadlock equilibrium z_{rd} given by (22).

CLAIM 23. *Let $J_0 = D_{z_r} f_r(z_r, \epsilon_v)|_{z_r=z_{rd}}$ be the Jacobian of (19) evaluated at the deadlock equilibrium defined by (22). Then*

$$J_0 = \begin{bmatrix} j_{11} & 0 & j_{13} & 0 \\ 0 & j_{22} & 0 & 0 \\ j_{31} & 0 & j_{33} & 0 \\ 0 & j_{42} & 0 & j_{44} \end{bmatrix}$$

where the non-zero components are given by

$$(38) \quad j_{11} = \frac{\partial \dot{\Delta} \varphi_r}{\partial \Delta \varphi_r} \Big|_{z_r=z_{rd}} = -16\eta^2 \bar{m}_{rd} / (1 + 4\eta^2)^{3/2},$$

$$(39) \quad j_{13} = \frac{\partial \dot{\Delta} \varphi_r}{\partial \Delta m_r} \Big|_{z_r=z_{rd}} = -2/\sqrt{1 + 4\eta^2},$$

$$(40) \quad j_{22} = \frac{\partial \dot{\varphi}_r}{\partial \bar{\varphi}_r} \Big|_{z_r=z_{rd}} = -8\bar{m}_{rd} / \sqrt{1 + 4\eta^2}$$

$$(41) \quad j_{31} = \frac{\partial \dot{\Delta} \dot{m}_r}{\partial \Delta \varphi_r} \Big|_{z_r=z_{rd}} = 4\epsilon_v \bar{m}_{rd} + (1 - 2\bar{m}_{rd})(1 + \bar{m}_{rd})/\epsilon_v$$

$$(42) \quad j_{33} = \frac{\partial \dot{\Delta} \dot{m}_r}{\partial \Delta \dot{m}_r} \Big|_{z_r=z_{rd}} = -2\epsilon_v + (1 - 2\bar{m}_{rd})/(2\epsilon_v)$$

$$(43) \quad j_{42} = \frac{\partial \dot{m}_r}{\partial \bar{\varphi}_r} \Big|_{z_r=z_{rd}} = 4\epsilon_v \bar{m}_{rd} + (1 - 2\bar{m}_{rd})(1 + \bar{m}_{rd})/\epsilon_v$$

$$\begin{aligned}
(44) \quad j_{44} &= \frac{\partial \dot{m}_r}{\partial \dot{m}_r} \Big|_{z_r=z_{rd}} = -2\epsilon_v + (1 - 2\bar{m}_{rd})/(2\epsilon_v) - 8\bar{m}_{rd} - (1 + \bar{m}_{rd})/\epsilon_v \\
&= -2(\epsilon_v + 4\bar{m}_{rd}) - (1 + 4\bar{m}_{rd})/(2\epsilon_v).
\end{aligned}$$

The characteristic polynomial $p_4(\lambda)$ of J_0 is given by the determinant $|J_0 - \lambda I|$, where I is the identity matrix. This determinant can be computed directly using expansion by minors:

$$(45) \quad p_4(\lambda) = |J_0 - \lambda I| = (\lambda - j_{22})(\lambda - j_{44})(\lambda^2 - (j_{11} + j_{33})\lambda + j_{11}j_{33} - j_{13}j_{31}).$$

Note that

$$\lim_{\eta \rightarrow 0} J_0 = J_1 = \begin{bmatrix} 0 & 0 & -2 & 0 \\ 0 & -8\bar{m}_{rd} & 0 & 0 \\ j_{31} & 0 & j_{33} & 0 \\ 0 & j_{42} & 0 & j_{44} \end{bmatrix}.$$

Similarly, $p_4(\lambda)$ reduces to

$$\lim_{\eta \rightarrow 0} p_4(\lambda) = (\lambda - j_{22})(\lambda - j_{44})(\lambda^2 - j_{33}\lambda + 2j_{31}).$$

B.2. Criticality of the Hopf bifurcation in Theorem 1. The following result concerns the the Hopf bifurcation whose existence is proven in Theorem 1. It implies that the Hopf bifurcation is supercritical, so the periodic solutions created by the bifurcation are stable limit cycles.

The remainder of this section constitutes the proof of Lemma 7. As in Appendix A, write $\ell_1|_{(z_0, \epsilon_0)} = \frac{1}{2\omega_0} \text{Re}[T_1 + T_2 + T_3]$, where, from (37),

$$\begin{aligned} T_1 &= \langle p, C(q, q, \bar{q}) \rangle \\ T_2 &= -2 \langle p, B(q, J_0^{-1} B(q, \bar{q})) \rangle \\ T_3 &= \langle p, B(\bar{q}, (2i\omega_0 I - J_0)^{-1} B(q, q)) \rangle, \end{aligned}$$

I is the identity matrix, and ω_0, p, q, B , and C are as defined in Appendix A. We show that $\text{Re}[T_i] < 0$ for each $i \in \{1, 2, 3\}$. Together, these imply that $\ell_1 < 0$, since $\omega_0 > 0$ by definition.

Let $J_0 = D_z f|_{(z_0, \epsilon_0)}$ be the Jacobian of the dynamics (19) evaluated at the bifurcation point and let $J_1 = \lim_{\eta \rightarrow 0} J_0$. As shown in (23), J_1 has two purely imaginary eigenvalues when $j_{33} = 4 - (1 - 2\bar{m}_{rd})/\epsilon_v^2 = 0$. This implies that $1 - 2\bar{m}_{rd} = 4\epsilon_v^2$ at the bifurcation point.

As shown in Claim 23, the limiting Jacobian $\lim_{\eta \rightarrow 0} J_0 = J_1$ can be computed in closed form and takes the value

$$(46) \quad \begin{aligned} J_1 &= \begin{bmatrix} 0 & 0 & -2 & 0 \\ 0 & j_{22} & 0 & 0 \\ j_{31} & 0 & j_{33} & 0 \\ 0 & j_{42} & 0 & j_{44} \end{bmatrix} \\ &= \begin{bmatrix} 0 & 0 & -2 & 0 \\ 0 & -8\bar{m}_{rd} & 0 & 0 \\ 8(1 - 2\epsilon_v^2)\epsilon_v & 0 & 0 & 0 \\ 0 & 4\epsilon_v(1 + 2\bar{m}_{rd}) & 0 & -8\bar{m}_{rd} - (1 + \bar{m}_{rd})/\epsilon_v \end{bmatrix}, \end{aligned}$$

where we have used the relationship established in (23) $1 - 2\bar{m}_{rd} = 4\epsilon_v^2$ that holds at the bifurcation point in the final expression.

The eigenvalue problems $J_1 q = i\omega_0 q$, $J_1^T p = -i\omega_0 p$ can be solved analytically, yielding

$$\omega_0 = \sqrt{2j_{31}},$$

$$q = [q_1 \ 0 \ q_3 \ 0]^T = \left[i\sqrt{\frac{2}{j_{31}}} \ 0 \ 1 \ 0 \right]^T,$$

$$p = [p_1 \ 0 \ p_3 \ 0]^T = \left[\frac{i}{2}\sqrt{\frac{j_{31}}{2}} \ 0 \ \frac{1}{2} \ 0 \right]^T.$$

The eigenvectors satisfy the required normalization condition $\langle p, q \rangle = 1$. The sparsity of p and q greatly simplifies the computations of T_1, T_2, T_3 .

B.2.1. Computing T_1 . First, we compute T_1 . Recall from (37) that $T_1 = \langle p, C(q, q, \bar{q}) \rangle$. Direct computation shows that $C_i(q, q, \bar{q}) = 0$ for $i \in \{1, 2, 4\}$. The relevant components of C_{3jkl} are $C_{3111} = 24\epsilon_v \bar{m}_{rd}$, $C_{3113} = C_{3131} = C_{3311} = -4\epsilon_v$. Substituting in the values of p and q then yields

$$T_1 = - \left(\frac{4\epsilon_v}{j_{31}} + 12\epsilon_v \bar{m}_{rd} \left(\frac{2}{j_{31}} \right)^{3/2} i \right)$$

$$\Rightarrow \text{Re}[T_1] = -\frac{4\epsilon_v}{j_{31}} = -\frac{1}{2 - 4\epsilon_v^2},$$

which is negative for all $\epsilon_v < \sqrt{2}/2 \approx 0.707$, including $\epsilon_v = \epsilon_{v,0} \approx 0.262$.

B.2.2. Computing T_2 . Next, we compute T_2 . Recall from (37) that $T_2 = -2\langle p, B(q, J_1^{-1}B(q, \bar{q})) \rangle$. Direct computation shows that $B_i(q, \bar{q}) = 0$ for $i \in \{1, 2, 3\}$ and that $B_4(q, \bar{q})$ has relevant terms $B_{411} = -4\epsilon_v \bar{m}_{rd}$, $B_{413} = B_{431} = 2\epsilon_v$, $B_{433} = 2$. Then $B_4(q, \bar{q}) = -4\epsilon_v \bar{m}_{rd} q_1 \bar{q}_1 + 2\epsilon_v q_1 q_3 + 2\epsilon_v \bar{q}_1 q_3 + 2q_3^2 = -\frac{8\epsilon_v \bar{m}_{rd}}{j_{31}} + 2$. The matrix J_1^{-1} can be computed from (46) in closed form, and is equal to

$$J_1^{-1} = \begin{bmatrix} 0 & 1/j_{31} & 0 & 0 \\ 0 & 1/j_{22} & 0 & 0 \\ -1/2 & 0 & 0 & 0 \\ 0 & -j_{42}/(j_{22}j_{44}) & 0 & 1/j_{44} \end{bmatrix},$$

where j_{kl} are defined in (46), so the only non-zero component of $J_1^{-1}B(q, \bar{q})$ is the fourth one, which is equal to $B_4(q, \bar{q})/j_{44} = (-\frac{8\epsilon_v \bar{m}}{j_{31}} + 2)/j_{44}$. Direct computation then shows that $B_i(q, J_1^{-1}B(q, \bar{q})) = 0$ for $i \in \{1, 2, 4\}$ and that $B_3(q, J_1^{-1}B(q, \bar{q})) = (-1/\epsilon_v + i(8\epsilon_v - 2(1 - \bar{m})/\epsilon_v)\sqrt{2/j_{31}})(-\frac{8\epsilon_v \bar{m}}{j_{31}} + 2)/j_{44}$ and therefore that

$$\begin{aligned} \text{Re}[T_2] &= \text{Re} \left[-2\langle p, B(q, J_1^{-1}B(q, \bar{q})) \rangle \right] = \frac{-\frac{8\epsilon_v \bar{m}}{j_{31}} + 2}{\epsilon_v j_{44}} \\ &= \frac{4\epsilon_v^2 - 3}{(2\epsilon_v^2 - 1)(32\epsilon_v^3 + 4\epsilon_v^2 - 8\epsilon_v - 3)}. \end{aligned}$$

It is clear that the two quadratic factors are both negative for all $\epsilon_v < \sqrt{2}/2 \approx 0.707$, including $\epsilon_v = \epsilon_{v,0} \approx 0.262$. The cubic factor can be shown to have one real-valued root at $\epsilon_v \approx 0.582$ and is negative for all values of ϵ_v less than the root, including $\epsilon_v = \epsilon_{v,0}$. Therefore, all three factors are negative when $\epsilon_v = \epsilon_{v,0}$ and $\text{Re}[T_2] < 0$.

B.2.3. Computing T_3 . Finally, we compute T_3 . Recall from (37) that $T_3 = \langle p, B(\bar{q}, (2i\omega_0 I - J_1)^{-1} B(q, q)) \rangle$. As in the case of T_2 , direct computation shows that $B_i(q, q) = 0$ for $i \in \{1, 2, 3\}$ and that $B_4(q, q)$ has relevant terms $B_{411}, B_{413} = B_{431}$, and B_{433} . Then $B_4(q, q) = 2 - 8\bar{m}_{rd}\epsilon_v/j_{31} + 4\epsilon_v\sqrt{2}/j_{31}i$.

Let $\Gamma = (2i\omega_0 I - J_1)^{-1}$, which has the structure

$$\Gamma = \begin{bmatrix} \gamma_{11} & 0 & \gamma_{13} & 0 \\ 0 & \gamma_{22} & 0 & 0 \\ \gamma_{31} & 0 & \gamma_{33} & 0 \\ 0 & \gamma_{42} & 0 & \gamma_{44} \end{bmatrix},$$

where $\gamma_{44} = 1/(-j_{44} + 2i\sqrt{2j_{31}}) = (-j_{44} - 2i\sqrt{2j_{31}})/(8j_{31} + j_{44}^2)$. The first three components $(\Gamma B(q, q))_i = 0$ for $i \in \{1, 2, 3\}$ and the only non-zero component is the fourth one given by $\gamma_{44}B_4(q, q)$. Then direct computation shows that $B_i(\bar{q}, \Gamma B(q, q)) = 0$ for $i \in \{1, 2, 4\}$ and that

$$B_3(\bar{q}, \Gamma B(q, q)) = (B_{314}\bar{q}_1 + B_{334})\gamma_{44}B_4(q, q),$$

where $B_{314} = 8\epsilon_v - 2(1 + \bar{m}_{rd})/\epsilon_v$ and $B_{334} = -1/\epsilon_v$. Therefore,

$$T_3 = p_3 \overline{B_3(\bar{q}, \Gamma B(q, q))} = \frac{(B_{314}\bar{q}_1 + B_{334})\gamma_{44}B_4(q, q)}{2}.$$

We proceed by bounding the real part of T_3 . Define the quantity $\delta_1 + \delta_2 i := (B_{314}\bar{q}_1 + B_{334})B_4(q, q)$, where $\delta_1, \delta_2 \in \mathbb{R}$. Direct computation using (23) shows that

$$\delta_1 = -\frac{5 - 48\epsilon_v^2 + 256\epsilon_v^4 - 640\epsilon_v^6 + 512\epsilon_v^8}{\epsilon_v(1 - 2\epsilon_v^2)},$$

$$\delta_2 = \frac{3 - 2\epsilon_v - 60\epsilon_v^2 + 480\epsilon_v^4 - 1536\epsilon_v^6 + 1536\epsilon_v^8}{\epsilon_v\sqrt{\epsilon_v - 2\epsilon_v^3}}.$$

It can be shown that $0 < \epsilon_v < 0.580$ implies that $\delta_1 < 0$ and that $0 < \epsilon_v < 0.280$ implies that $\delta_2 > 0$. The bifurcation value of $\epsilon_{v,0} \approx 0.262$ satisfies both of these sufficient conditions.

Recall from above that

$$\gamma_{44} = \frac{-j_{44} - 2i\sqrt{2j_{31}}}{8j_{31} + j_{44}^2}.$$

Then the real part of T_3 can be expressed as

$$(47) \quad \text{Re}(T_3) = \frac{-\delta_1 j_{44} + 2\delta_2 \sqrt{2j_{31}}}{2(8j_{31} + j_{44}^2)}.$$

It is clear that $j_{31} > 0$ for $\epsilon_v < \sqrt{2}/2$, so at the critical value $\epsilon_{v,0} \approx 0.262$ the denominator of (47) is positive. Therefore, $\text{Re}(T_3) < 0$ if the numerator $-\delta_1 j_{44} + 2\delta_2 \sqrt{2j_{31}} < 0$. Using (23) to express the numerator in terms of ϵ_v , we get

$$(48) \quad -\delta_1 j_{44} + 2\delta_2 \sqrt{2j_{31}} = \frac{f(\epsilon_v)}{-2\epsilon_v^2(1 - 2\epsilon_v^2)},$$

where

$$(49) \quad f(\epsilon_v) = 15 - 8\epsilon_v - 132\epsilon_v^2 + 512\epsilon_v^3 + 896\epsilon_v^4 - 6016\epsilon_v^5 - 2944\epsilon_v^6 \\ + 26624\epsilon_v^7 + 4096\epsilon_v^8 - 49152\epsilon_v^9 - 2048\epsilon_v^{10} + 32768\epsilon_v^{11}.$$

It is clear that $-2\epsilon_v^2(1 - 2\epsilon_v^2) < 0$ for $\epsilon_v < \sqrt{2}/2$, so $\text{Re}[T_3] < 0$ if $f(\epsilon_v) > 0$. It can be shown that $f(\epsilon_v)$ has one real-valued root at $\epsilon_v \approx -0.568$ and is positive for all values of ϵ_v greater than this root. Therefore, $f(\epsilon_v) > 0$ for all positive ϵ_v , which implies that $\text{Re}(T_3) < 0$.

Combining the results for T_1, T_2 , and T_3 , we get that

$$\text{Re}(T_1) + \text{Re}(T_2) + \text{Re}(T_3) < 0,$$

which implies that

$$\begin{aligned} \ell_1|_{(x_0, \mu_0)} &= \frac{1}{2\omega_0} \text{Re}(T_1 + T_2 + T_3) \\ &= \frac{1}{2\omega_0} (\text{Re}(T_1) + \text{Re}(T_2) + \text{Re}(T_3)) < 0, \end{aligned}$$

the desired result.

Appendix C. A tutorial on geometric singular perturbation theory.

Singular perturbation theory is a tool for studying dynamical systems characterized by two time scales, slow time t and fast time τ . The time scales are related by $\tau = t/\epsilon$, where $\epsilon > 0$ is a small parameter. In the slow time scale, the dynamical system is governed by differential equations that are singular at $\epsilon = 0$. By taking the limit $\epsilon \rightarrow 0$, i.e., assuming that the fast dynamics are much faster than the slow dynamics, one can often reduce a system to the slow dynamics.

Fenichel did fundamental work on this theory, for which [6] is a relatively comprehensive reference. Of particular interest to this paper is the theory he developed that allows one to relate the behavior of (the invariant manifolds of) a system in the limit $\epsilon \rightarrow 0$ to the behavior with finite $\epsilon > 0$. In order to do this globally on a compact subset of the state space, Fenichel developed a geometric, or coordinate-free, notion of singular perturbation. The remainder of the section constitutes a summary of the relevant material in [6]. We begin by summarizing the local results, which are expressed in a given set of coordinates, before introducing the more abstract global, coordinate-free results.

C.1. Local results. Let M be an open subset of $\mathbb{R}^\mu \times \mathbb{R}^\nu$, and let $\mathcal{E} = M \cap (\mathbb{R}^\mu \times \{0\})$ be nonempty. We consider a system of the form

$$(50) \quad \begin{aligned} \dot{x} &= f_0(x, y, \epsilon) \\ \epsilon \dot{y} &= g(x, y, \epsilon) \end{aligned}$$

where $\dot{\cdot}$ denotes differentiation with respect to t , defined for $(x, y) \in M$, for small, real ϵ . When $\epsilon = 0$ the system (50) degenerates to the reduced system

$$(51) \quad \begin{aligned} \dot{x} &= f_0(x, y, 0) \\ 0 &= g(x, y, 0). \end{aligned}$$

The second equation of (51) is an implicit function that defines y as a function of x . The relation can be expressed explicitly, at least locally, as a function $y = h(x)$ [11]. The set $\{(x, y) | y = h(x)\}$ is called the *slow manifold*. By translating the y coordinates by $-h(x)$, we can set $y = 0$ on the slow manifold, which we denote by \mathcal{E} . Therefore, we assume that

$$(52) \quad g(x, 0, 0) = 0 \quad \text{for all } (x, 0) \in \mathcal{E},$$

so that (51) defines a flow in \mathcal{E} , and we assume that this flow has a periodic orbit $\gamma_0 : x = p(t), y = 0$. Fenichel's aim is to describe the orbit structure of (50) for small nonzero ϵ .

By rescaling time to $\tau = t/\epsilon$, we can transform (50) to

$$(53) \quad \begin{aligned} x' &= \epsilon f_0(x, y, \epsilon) \\ y' &= g(x, y, \epsilon), \end{aligned}$$

where $'$ denotes differentiation with respect to τ . The set \mathcal{E} consists entirely of equilibrium points of the system (53) in the limit $\epsilon \rightarrow 0$.

The plan is to relate the orbit structure of (50) near γ_0 , for small nonzero ϵ , to the orbit structure of the reduced system (51) near γ_0 and to the linearization of $\lim_{\epsilon \rightarrow 0}$ (53) at points of γ_0 . The linearization of $\lim_{\epsilon \rightarrow 0}$ (53) at $(x, 0) \in \mathcal{E}$ is

$$(54) \quad \begin{bmatrix} \delta x \\ \delta y \end{bmatrix}' = \begin{bmatrix} 0 & 0 \\ 0 & D_2g(x, 0, 0) \end{bmatrix} \begin{bmatrix} \delta x \\ \delta y \end{bmatrix},$$

where $D_2g(x, 0, 0)$ denotes differentiation with respect to the second argument of g evaluated at $(x, 0, 0)$. The second component satisfies

$$(55) \quad \delta y' = D_2g(x, 0, 0)\delta y,$$

a linear equation parametrized by $(x, 0) \in \mathcal{E}$. We refer to (55) (Equation (3.8) of [6]) as the *initial layer equation*.

The first qualitative question that Fenichel asks about (50) is whether it has a periodic orbit γ_ϵ near γ_0 for ϵ near zero. Fenichel [6] claimed that Anosov [1] obtained the most general result in the literature. In particular [6, Section III], Anosov proved that γ_0 can be continued to a family γ_ϵ if: (i) γ_0 , regarded as a periodic orbit of the reduced system (51), has 1 as a Floquet multiplier of multiplicity precisely one, and (ii) for each $(x, 0) \in \gamma_0$, the initial layer equation (55) has a hyperbolic equilibrium point at $\delta y = 0$. The first condition can be interpreted as a nondegeneracy requirement on the periodic orbit γ_0 itself, while the second condition is sometimes called normal hyperbolicity of the slow manifold defined by $g(x, y, 0) = 0$. Theorem 13.1 of [6] makes this result precise.

C.2. Global results. The definitions up to here have been in a given set of coordinates. In order to properly account for limit cycles, Fenichel develops a global, coordinate-free notion of the singular perturbation problem. Let M be a C^{r+1} manifold, $1 \leq r \leq \infty$. Let $X^\epsilon : M \rightarrow TM$ be a family of vector fields on M , parametrized by $\epsilon \in (-\epsilon_0, \epsilon_0)$, such that X^ϵ is a C^r function of (m, ϵ) . Let \mathcal{E} be a C^r submanifold of M consisting entirely of equilibrium points of X^0 , and let $z = \phi(m)$ be a C^{r+1} local coordinate in M . In z -coordinates the flow of X^ϵ satisfies

$$(56) \quad z' = X^\epsilon \phi(\phi^{-1}(z))$$

subject to the condition

$$X^\epsilon \phi(\phi^{-1}(z)) = 0 \quad \text{for } z \in \phi(\mathcal{E}).$$

Let μ be the dimension of \mathcal{E} and let ν be the codimension of \mathcal{E} in M . Because X^0 vanishes identically on \mathcal{E} , $T_m\mathcal{E}$ is in the kernel of $TX^0(m)$ for any $m \in M$. In coordinates, then, $Tx^0(m)$ will have μ eigenvalues equal to zero and ν additional

eigenvalues, which we call the *nontrivial eigenvalues*. The subspace $T_m\mathcal{E}$ is invariant under $TX^0(m)$, and so $TX^0(m)$ induces a linear map

$$QX^0(m) : T_mM/T_m\mathcal{E} \rightarrow T_mM/T_m\mathcal{E}$$

on the quotient space. The eigenvalues of $QX^0(m)$ are the nontrivial eigenvalues of the linearization of $\lim_{\epsilon \rightarrow 0}$ (56) at $z = \phi(m)$.

Let \mathcal{E}_R be the open set where QX^0 is invertible. For each $m \in \mathcal{E}_R$, $T_m\mathcal{E}$ has a unique complement N_m which is invariant under $TX^0(m)$. Let $\pi^\mathcal{E}$ denote the projection on $T\mathcal{E}$ defined by the splitting $TM|_{\mathcal{E}_R} = T\mathcal{E} \oplus N$. Let $\mathcal{E}_H \subset \mathcal{E}_R$ be the open subset where QX^0 has no pure imaginary eigenvalues; this is the normally-hyperbolic component of the slow manifold.

In \mathcal{E}_R the reduced vector field X_R is defined by

$$(57) \quad X_R(m) = \pi^\mathcal{E} \partial / \partial \epsilon X^\epsilon(m)|_{\epsilon=0}.$$

Now we can state the main theorem that asserts conditions under which periodic orbits of the reduced vector field X_R defined in the limit $\epsilon \rightarrow 0$ persist for $\epsilon > 0$.

THEOREM 24 ([6, Theorem 13.1]). *Let M be a C^{r+1} manifold, $2 \leq r \leq \infty$. Let $X^\epsilon, \epsilon \in (-\epsilon_0, \epsilon_0)$ be a C^r family of vector fields, and let \mathcal{E} be a C^r submanifold of M consisting entirely of equilibrium points of X^0 . Let $\gamma \in \mathcal{E}_H$ be a periodic orbit of the reduced vector field X_R , and suppose that γ_0 , as a periodic orbit of X_R , has 1 as a Floquet multiplier of multiplicity precisely one. Then there exists $\epsilon_1 > 0$ and there exists a C^{r-1} family of closed curves $\gamma_\epsilon, \epsilon \in (-\epsilon_1, \epsilon_1)$, such that $\gamma_0 = \gamma$ and γ_ϵ is a periodic orbit of $\epsilon^{-1}X^\epsilon$. The period of γ_ϵ is a C^{r-1} function of ϵ .*

For many applications, we are only interested in the case of small positive ϵ . In [6, Section V], Fenichel explains how he is able to obtain results for $\epsilon \in (-\epsilon_0, \epsilon_0)$. Furthermore, the stability results of [6, Theorem 13.2] are stated for $\epsilon > 0$. Let us now discuss how the theorem is applied. The main conditions are 1) that the periodic orbit γ_0 be contained in \mathcal{E}_H , the normally-hyperbolic component of the slow manifold, and 2) that γ_0 have 1 as a Floquet multiplier of multiplicity precisely one.

If one has a global coordinate system for \mathcal{E} , testing for normal hyperbolicity reduces to verifying that the eigenvalues of $\partial g / \partial y|_{\mathcal{E}}$ have non-zero real parts; if the real parts are negative, \mathcal{E} is stable. The Floquet multipliers of γ_0 are the eigenvalues of B , the linearized Poincaré map of γ_0 , so a multiplier of 1 corresponds to a fixed point of the Poincaré map, and multipliers less than (greater than) 1 correspond to stability (instability) of the orbit. There are μ Floquet multipliers $\rho_i, i \in \{1, \dots, \mu\}$, where μ is the dimension of \mathcal{E} . It can be shown [8] that $\det(B) = \prod_{i=1}^{\mu} \rho_i = \exp \int_0^T \text{tr}(A(s)) ds$, where T is the period of the periodic orbit and $A(s)$ is the linearization of the reduced dynamics $Df(x, 0, 0)|_{\gamma_0(s)}$. The existence of the periodic orbit means that there is one Floquet multiplier equal to 1. In general, ρ_i have to be found by numerically computing B , unless one can bound the sign of $\text{tr} A$ on the slow manifold. Alternatively, if one can show that the limit cycle is asymptotically stable on the slow manifold, the Floquet multiplier condition follows.

Acknowledgement. This work was supported in part by Air Force Research Laboratory grant FA865015D1845 (subcontract 669737-1).

REFERENCES

- [1] D. V. Anosov. On limit cycles in systems of differential equations with a small parameter in the highest derivatives. *AMS Translations*, Ser. 2(33):233–275, 1963.
- [2] S. M. Baer and T. Erneux. Singular Hopf bifurcation to relaxation oscillations. *SIAM Journal on Applied Mathematics*, 46(5):721–739, 1986.
- [3] R. Bogacz, E. Brown, J. Moehlis, P. Holmes, and J. D. Cohen. The physics of optimal decision making: a formal analysis of models of performance in two-alternative forced-choice tasks. *Psychological review*, 113(4):700, 2006.
- [4] R. R. Burridge, A. A. Rizzi, and D. E. Koditschek. Sequential composition of dynamically dexterous robot behaviors. *The International Journal of Robotics Research*, 18(6):534–555, 1999.
- [5] A. De and D. E. Koditschek. Parallel composition of templates for tail-energized planar hopping. In *2015 IEEE International Conference on Robotics and Automation (ICRA)*, pages 4562–4569, May 2015.
- [6] N. Fenichel. Geometric singular perturbation theory for ordinary differential equations. *Journal of Differential Equations*, 31(1):53–98, 1979.
- [7] J. Guckenheimer. Bifurcations of relaxation oscillations. *Normal Forms, Bifurcations and Finiteness Problems in Differential Equations*, pages 295–316, 2004.
- [8] J. Guckenheimer and P. J. Holmes. *Nonlinear oscillations, dynamical systems, and bifurcations of vector fields*, volume 42 of *Applied Mathematical Sciences*. Springer Science & Business Media, 2013.
- [9] J. Hofbauer and K. Sigmund. *Evolutionary games and population dynamics*. Cambridge University Press, 1998.
- [10] C. L. Hull. *Principles of Behavior*. Appleton-Century-Crofts, New York, 1943.
- [11] C. K. R. T. Jones. Geometric singular perturbation theory. In *Dynamical systems*, volume 1609 of *Lecture Notes in Mathematics*, pages 44–118. Springer, 1995.
- [12] H. K. Khalil. *Nonlinear systems*. Prentice Hall, 3 edition, 2002.
- [13] D. E. Koditschek. The application of total energy as a Lyapunov function for mechanical control systems. *Contemporary Mathematics*, February 1989.
- [14] H. Kress-Gazit, G. E. Fainekos, and G. J. Pappas. Temporal-logic-based reactive mission and motion planning. *IEEE Transactions on Robotics*, 25(6):1370–1381, 2009.
- [15] Y. A. Kuznetsov. *Elements of applied bifurcation theory*, volume 112. Springer Science & Business Media, 1998.
- [16] J. LaSalle. Stability theory for ordinary differential equations. *Journal of Differential Equations*, 4(1):57–65, 1968.
- [17] N. E. Leonard, T. Shen, B. Nabet, L. Scardovi, I. D. Couzin, and S. A. Levin. Decision versus compromise for animal groups in motion. *Proceedings of the National Academy of Sciences*, 109(1):227–232, 2012.
- [18] W. G. Mitchener and M. A. Nowak. Chaos and language. *Proceedings of the Royal Society of London-B*, 271(1540):701–704, 2004.
- [19] D. Pais, C. H. Caicedo-Núñez, and N. E. Leonard. Hopf bifurcations and limit cycles in evolutionary network dynamics. *SIAM Journal on Applied Dynamical Systems*, 11(4):1754–1784, 2012.
- [20] D. Pais, P. M. Hogan, T. Schlegel, N. R. Franks, N. E. Leonard, and J. A. Marshall. A mechanism for value-sensitive decision-making. *PloS one*, 8(9):e73216, 2013.
- [21] H. L. Petri and J. M. Govern. *Motivation: Theory, research, and application*. Cengage Learning, 2012.
- [22] E. Rimon and D. E. Koditschek. Exact robot navigation using artificial potential fields. *IEEE Transactions on Robotics and Automation*, 8(5):501–518, 1992.
- [23] H. Royden and P. Fitzpatrick. *Real Analysis*. Boston, MA: Prentice Hall, 4th edition, 2010.
- [24] T. D. Seeley, P. K. Visscher, T. Schlegel, P. M. Hogan, N. R. Franks, and J. A. Marshall. Stop signals provide cross inhibition in collective decision-making by honeybee swarms. *Science*, 335(6064):108–111, 2012.
- [25] D. D. Sokolov. Elliptic coordinates. In *Encyclopedia of Mathematics*. Springer, 2011.
- [26] R. S. Woodworth. *Dynamic Psychology*. Columbia University Press, 1918.